© 2020. Published by The Company of Biologists Ltd | Journal of Cell Science (2020) 133, jcs235994. doi:10.1242/jcs.235994

RESEARCH ARTICLE

Pseudohyphal growth in *Saccharomyces cerevisiae* involves protein kinase-regulated lipid flippases

Merethe Mørch Frøsig[1], Sara Rute Costa[1], Johannes Liesche[1,*], Jeppe Thulin Østerberg[1], Susanne Hanisch[1], Sebastian Nintemann[1], Helle Sørensen[2], Michael Palmgren[1], Thomas Günther Pomorski[1,3] and Rosa L. López-Marqués[1,‡]

ABSTRACT

Lipid flippases of the P4 ATPase family establish phospholipid asymmetry in eukaryotic cell membranes and are involved in many essential cellular processes. The yeast *Saccharomyces cerevisiae* contains five P4 ATPases, among which Dnf3p is poorly characterized. Here, we demonstrate that Dnf3p is a flippase that catalyzes translocation of major glycerophospholipids, including phosphatidylserine, towards the cytosolic membrane leaflet. Deletion of the genes encoding Dnf3p and the distantly related P4 ATPases Dnf1p and Dnf2p results in yeast mutants with aberrant formation of pseudohyphae, suggesting that the Dnf1p–Dnf3p proteins have partly redundant functions in the control of this specialized form of polarized growth. Furthermore, as previously demonstrated for Dnf1 and Dnf2p, the phospholipid flipping activity of Dnf3p is positively regulated by flippase kinase 1 (Fpk1p) and Fpk2p. Phylogenetic analyses demonstrate that Dnf3p belongs to a subfamily of P4 ATPases specific for fungi and are likely to represent a hallmark of fungal evolution.

KEY WORDS: Polarized growth, Cell budding, Pseudohyphal growth, Lipid flippase, Flippase kinase

INTRODUCTION

Cellular membranes separate cells from the environment and allow for compartmentalization of different processes inside cells. Many membranes present a characteristic asymmetric phospholipid distribution between the two leaflets necessary for their physiological function (Sebastian et al., 2012; Zachowski, 2012). To achieve such transbilayer lipid asymmetry, phospholipids are actively transported across the bilayer at the expense of ATP (van Meer, 2011). P4 ATPases or flippases are integral membrane proteins responsible for phospholipid transport towards the cytosolic side of biological membranes (López-Marqués et al., 2011). P4 ATPase-dependent regulation of lipid asymmetry is essential for cell survival, as it affects membrane stability and impermeability, cell polarity, apoptotic cell recognition, cell division and regulation of membrane protein function (López-Marqués et al., 2014).

In *Saccharomyces cerevisiae*, the family of P4 ATPases comprises five members: Drs2p, Neo1p, Dnf1p, Dnf2p and Dnf3p. Drs2p is a well-characterized lipid flippase that functions in the trans-Golgi network (TGN) and is specific for phosphatidylserine (PS) and phophatidylethanolamine (PE) (Chen et al., 1999; Saito et al., 2004). Drs2p-catalyzed flipping of PS and PE creates membrane curvature and serves as a signal to attract proteins involved in vesicle transport, and both processes contribute to secretory vesicle formation (Xu et al., 2013). Neo1p performs an essential role in vesicle transport between the endoplasmic reticulum (ER) and Golgi, and has been shown to affect the asymmetric distribution of mainly PE, but also PS, at the plasma membrane through an as yet unclear mechanism (Hua and Graham, 2003; Takar et al., 2016; Wicky et al., 2004; Wu et al., 2016). Dnf1p and Dnf2p localize the plasma membrane, where they primarily transport phosphatidylcholine (PC) and PE, as well as the corresponding lysophospholipids and glycosphingolipids (Baldridge et al., 2013; Furuta et al., 2007; Hachiro et al., 2013; Pomorski et al., 2003; Riekhof and Voelker, 2006, 2009; Saito et al., 2004; Roland et al., 2019). Like Drs2p and Neo1p, Dnf1p and Dnf2p are required for vesicle transport in the late secretory and endocytic pathways (Hachiro et al., 2013; Hua et al., 2002; Pomorski et al., 2003).

Dnf3p is distantly related to other P4 ATPases in yeast, and is the least characterized P4 ATPase in this model organism. Dnf3p has been identified in intracellular membrane structures that most likely represent the TGN and early endosomes, and was proposed to colocalize with Drs2p (Pomorski et al., 2003). In contrast to Drs2p, Dnf3p has been reported to translocate primarily PC and PE (Alder-Baerens et al., 2006). Dnf3p activity contributes to vesicle formation (Hua et al., 2002) and vacuolar pH maintenance (Brett et al., 2011) but, due to its low level of expression, it has been suggested that Dnf3p only plays a minor role in the basal cell functions of *S. cerevisiae* (Furuta et al., 2007; Hua et al., 2002; Saito et al., 2004). However, during shmoo formation in the early phases of yeast mating, Dnf3p has been observed accumulating at the plasma membrane in the emerging tip (Sartorel et al., 2015). Interestingly, in the emerging tip, PS is being concentrated in the inner leaflet of the plasma membrane (Fairn et al., 2011). Members of the Dnf3p protein family in pathogenic filamentous fungi are strictly required for filamentous growth and penetration into the host cell (Balhadère and Talbot, 2001; Gilbert et al., 2006; Schultzhaus et al., 2019). This suggests that the Dnf3 protein family in fungi serves a general function in polarized growth.

[1]Department of Plant and Environmental Sciences, University of Copenhagen, Thorvaldsensvej 40, DK - 1871 Frederiksberg C, Denmark. [2]Data Science Lab, Department of Mathematical Sciences, University of Copenhagen, Universitetsparken 5, 2100 København Ø, Denmark. [3]Department of Molecular Biochemistry, Faculty of Chemistry and Biochemistry, Ruhr University Bochum, Bochum, Germany.
*Present address: College of Life Sciences, Northwest A&F University, Taicheng Road 3, 712100 Yangling, China.

‡Author for correspondence (rlo@plen.ku.dk)

S.R.C., 0000-0003-4402-6176; J.L., 0000-0001-8753-4037; J.T.Ø., 0000-0002-6481-9977; S.N., 0000-0001-9927-2601; H.S., 0000-0001-5273-6093; M.P., 0000-0002-9982-6114; T.G.P., 0000-0002-4889-0829; R.L.L., 0000-0002-5663-7903

Handling Editor: David Stephens
Received 11 July 2019; Accepted 1 July 2020

Journal of Cell Science (2020) 133, jcs235994. doi:10.1242/jcs.235994

A previous study demonstrated that Dnf3p can be phosphorylated *in vivo* by two kinases, flippase kinase 1 and 2 (Fpk1p and Fpk2p) (Nakano et al., 2008), but the physiological relevance of this process was not studied. Notably, Dnf1p and Dnf2p are activated through direct phosphorylation by Fpk1p and Fpk2p (Nakano et al., 2008). Unexpectedly, deletion of the β-subunit for Dnf1p and Dnf2p, Lem3p, does not exactly mimic the *fpk1Δ fpk2Δ* mutant phenotype (Nakano et al., 2008), although both genetic modifications should specifically result in lack of Dnf1p and Dnf2p flippase activity at the plasma membrane. Transport of PS across the yeast plasma membrane is only minimally affected in a *dnf1Δ dnf2Δ* double deletion mutant (Hachiro et al., 2013; Pomorski et al., 2003; Stevens et al., 2008) and in a *lem3* deletion mutant, which lacks the β-subunit of Dnf1p and Dnf2p (Kato et al., 2002), suggesting that an alternative PS transport system exists at the plasma membrane.

In this work, we tested the involvement of Dnf3p in flippase-kinase-mediated PS uptake at the plasma membrane in *S. cerevisiae* and examined the putative role for this protein in polarized pseudohyphal growth.

RESULTS

Dnf3p transports endogenous PS

Several lines of evidence suggest that a PS transport system distinct from Dnf1p and Dnf2p exists at the plasma membrane of *S. cerevisiae* (Hachiro et al., 2013; Nakano et al., 2008; Stevens et al., 2008). It was suggested that this system might be Drs2p, since this protein is known to recycle through the endocytic recycling pathway (Alder-Baerens et al., 2006; Saito et al., 2004). However, confirmation of this hypothesis is lacking. To investigate this, we analyzed the uptake of fluorescent nitrobenzoxadiazole (NBD) acyl-labeled lipid reporters by yeast cells lacking *DNF3* alone or *DNF1* and *DNF2*, alone or in combination with *DNF3* or *DRS2* (Fig. 1A). As expected, deletion of *DNF1* and *DNF2* resulted in a decrease of lipid uptake for fluorescently labeled PS, PE and PC. Further removal of Drs2p or Dnf3p did not significantly affect transport of NBD–PS, –PE, or –PC, confirming that Dnf1p and Dnf2p are the main contributors to lipid uptake at the plasma membrane. However, deletion of *DNF3* alone resulted in a reduction of lipid transport to ∼50–60% of

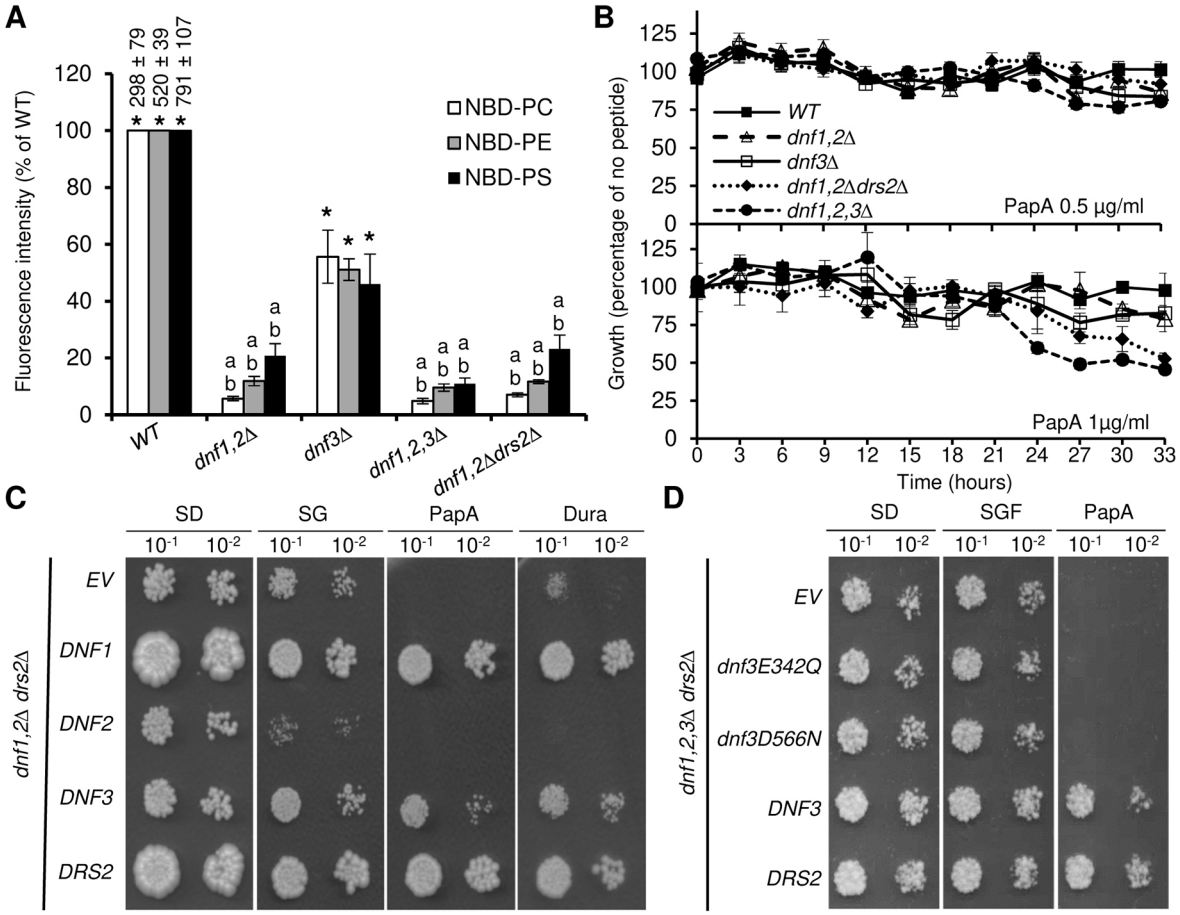

Fig. 1. Dnf3p is involved in phospholipid uptake and maintenance of plasma membrane PS asymmetry. (A) Yeast strains bearing deletions in the indicated genes were tested for uptake of NBD-lipids. Results are mean±s.e.m. from at least three biological replicates. Numbers above the bars represent geometric mean±s.e.m. of fluorescence values in arbitrary units. a, statistically significant (P<0.01) with respect to the wild type; b, statistically significant (P<0.01) with respect to *dnf3Δ*; *, statistically different (P<0.01) from all other strains (two-way ANOVA followed by Tukey confidence test). (B) Yeast strains bearing deletions in the indicated genes were grown in SD medium supplemented with papuamide A (PapA) at the indicated concentrations. Values are mean ±s.e.m. of three independent experiments. (C) Yeast *dnf1,2,3Δdrs2Δ* cells transformed with either empty vector (EV) or expression plasmids carrying wild-type *DNF1*, *DNF2*, *DNF3* or *DRS2* were spotted in two serial dilutions onto control plates with glucose (SD) or on galactose-containing plates (SG, induced expression), supplemented with PapA or the cytotoxic PE-binding peptide duramycin (Dura) as indicated. (D) Yeast *dnf1,2,3Δdrs2Δ* cells transformed with either empty vector (EV) or expression plasmids carrying wild-type *DNF3*, inactive versions of *DNF3 (dnf3E342Q, dnf3D566N),* or wild-type *DRS2* were grown on control plates with glucose (SD) or on galactose/fructose-containing plates (SGF, induced expression), supplemented with PapA as indicated. Numbers in C and D indicate cell dilutions.

Journal of Cell Science

Journal of Cell Science (2020) 133, jcs235994. doi:10.1242/jcs.235994

wild-type levels for all lipids tested, with the strongest effect for NBD–PS.

Transport of PC and PE by Dnf3p has previously been reported (Alder-Baerens et al., 2006). To test whether the observed PS translocation is directly caused by Dnf3p activity, we evaluated PS asymmetry at the plasma membrane in yeast mutants lacking different flippase combinations and grown in the presence of small concentrations of the PS-binding peptide papuamide A (Andjelic et al., 2008), which causes cytolysis and cell death by binding to extracellularly exposed PS (Parsons et al., 2006). PS sequestration in the cytosolic leaflet of the plasma membrane due to P4 ATPase-mediated internalization provides wild-type yeast cells with a natural resistance to this peptide. At lower peptide concentrations, growth of all yeast strains was similar to that of the wild type (Fig. 1B). By contrast, at a 1 µg/ml concentration of the peptide, the triple *dnf1,2,3*Δ and *dnf1,2*Δ*drs2*Δ mutant strains were more sensitive than *dnf1,2*Δ or *dnf3*Δ, which showed a similar growth to the wild type, suggesting that both Drs2p and Dnf3p are contributing to the plasma membrane PS asymmetry. In addition, the triple *dnf1,2,3*Δ mutant shows sensitivity to the drug at earlier times (24–27 h) than the *dnf1,2*Δ*drs2*Δ mutant, suggesting that the contribution of Dnf3p to PS asymmetry is stronger than that of Drs2p.

We have previously used a triple *dnf1,2*Δ*drs2*Δ mutant strain to characterize the lipid specificity of heterologously expressed flippases, due to its low background for lipid translocation (Jensen et al., 2016a,b). Overexpression of *DNF1*, *DNF3* or *DRS2* in this strain under the control of a strong galactose-inducible promoter resulted in yeast growth on plates containing papuamide A (Fig. 1C), confirming that all proteins can transport PS. Overexpression of *DNF2* seemed to be toxic for the yeast cells. We next employed a yeast strain lacking *DNF1*, *DNF2*, *DNF3*, and *DRS2*, which is devoid of all P4 ATPases shown so far to be directly involved in lipid translocation. This strain has very limited growth, but it is still viable in our yeast background. Growth of the *dnf1,2,3Δdrs2Δ* mutant was highly sensitive to papuamide A and this phenotype could be complemented by overexpression of *DRS2* (Fig. 1D). Confirming our previous results, expression of *DNF3* also resulted in complementation of the peptide-sensitive phenotype (Fig. 1D). To confirm that functional complementation requires an active Dnf3p, we generated two catalytically inactive variants, *dnf3E342Q* and *dnf3D566N*. While the *dnf3D566N* mutant lacks the conserved aspartic acid residue phosphorylated during the P-type ATPase catalytic cycle, the *dnf3E342Q* mutant lacks the glutamic acid residue in the conserved DGET-motif in P4 ATPases (TGES in other P-type ATPases) required for dephosphorylation (Anthonisen et al., 2006; Lenoir et al., 2009). Both catalytically inactive mutants were unable to support growth of the *dnf1,2,3Δdrs2Δ* strain on papuamide A (Fig. 1B). Taken together, our results demonstrate that active Dnf3p is indeed capable of promoting endogenous PS transport, in addition to that of PC and PE.

To test whether Dnf3p can reach the plasma membrane under our experimental conditions, we reinvestigated its intracellular localization. We chromosomally tagged the endogenous copy of *DNF3* with a SNAP tag at the C-terminal end of the protein in a wild-type yeast strain. The SNAP tag reacts specifically and rapidly with benzylguanine derivatives, allowing for the attachment of virtually any fluorophore after protein expression. Microscopy analysis of fluorescently labeled cells expressing Dnf3p–SNAP revealed numerous cells with a punctate staining pattern of endomembrane structures, in line with previous reports (Fig. S1A, panel I,II) (Hua et al., 2002; Pomorski et al., 2003). However, a large proportion of the cell culture displayed a ring-like peripheral staining pattern characteristic of plasma membrane localization (Fig. S1A, panel I,II). This localization was not an artifact of our labeling procedure, as we could not detect any plasma membrane signal for the actin-binding protein Abp1p, which under the conditions of our experiments resides solely in endomembranes (Fig. S1A, panel III) (Stagge et al., 2013).

To further characterize the plasma membrane localization of Dnf3p–SNAP, we incubated fluorescently labeled yeast cells with Trypan Blue to stain the cell wall (Liesche et al., 2015). This allowed for classification of cells into four different states related to their progression through the cell cycle, with State 1 corresponding to non-budding cells and State 4 corresponding to cells approaching cytokinesis (Fig. S1B). In non-budding cells (State 1), a Dnf3p–SNAP signal in endomembranes was evident in half of the population, whereas the other half showed a signal in the plasma membrane (Fig. S1B). During the initial stages of bud emergence (State 2), Dnf3p was confined to endomembranes, but located primarily to the plasma membrane during the isotropic bud growth phase and in cells approaching cytokinesis (States 3 and 4) (Fig. S1B). While we cannot rule out that vesicles containing Dnf3p are redirected to the plasma membrane in response to electroporation damage during fluorescent dye delivery, the capacity of Dnf3p to reach the plasma membrane in yeast has already been demonstrated during yeast mating (Sartorel et al., 2015), which is a cell-cycle-controlled process. Taken together, our results suggest that Dnf3p might reach the plasma membrane at certain time points during the cell cycle, and is therefore likely to be responsible for the residual PS-translocating activity at the plasma membrane detected in the *dnf1,2Δ* and *lem3Δ* mutants.

Overexpression of *FPK1* or *FPK2* induces Dnf3p-dependent PS transport

Given that flippase kinases Fpk1p and Fpk2p activate plasma membrane phospholipid flipping by Dnf1p and Dnf2p (Nakano et al., 2008), we wondered whether they also regulated Dnf3p activity. To study this, we used a *fpk1,2Δ* yeast strain to generate an *fpk1,2Δdnf1,2Δ* quadruple mutant lacking both the flippase kinases Dnf1p and Dnf2p. Overexpression of either Fpk1p or Fpk2p in the *fpk1,2Δ* strain induced translocation of fluorescent NBD–PC, –PE and –PS to the inner leaflet of the plasma membrane (Fig. 2A). Overexpression of the kinases in the *fpk1,2Δdnf1,2Δ* quadruple mutant increased uptake of labeled PC and especially PS (Fig. 2B). These findings indicate the presence of an Fpk1p- and Fpk2p-regulated system for PS transport at the yeast plasma membrane that is independent of Dnf1p and Dnf2p.

To test whether the observed Dnf1p- and Dnf2p-independent transport of NBD–PS is a result of Drs2p or Dnf3p activity, we attempted to create knockouts of *DRS2* or *DNF3* in the quadruple *fpk1,2Δdnf1,2Δ* mutant background. A deletion of *CDC50*, encoding the β-subunit of Drs2p, is synthetically lethal when combined with deletion of *FPK1* (Nakano et al., 2008), which might explain why we were not able to create a quintuple *fpk1,2Δdnf1,2Δdrs2Δ* mutant. However, we succeeded in deleting *DNF3* in the quadruple mutant background and in this way obtained a quintuple *fpk1,2Δdnf1,2,3Δ* mutant strain (henceforth termed *quint*).

We next compared phospholipid transport across the plasma membrane of the *quint* mutant with that of wild-type yeast and its parental strains *fpk1,2Δ* and *fpk1,2Δdnf1,2Δ*. In *fpk1,2Δ* cells, lipid transport was drastically reduced (by ∼80%) for all three NBD-labeled lipids tested (NBD–PC, –PE and –PS) (Fig. 2C). For

Journal of Cell Science (2020) 133, jcs235994. doi:10.1242/jcs.235994

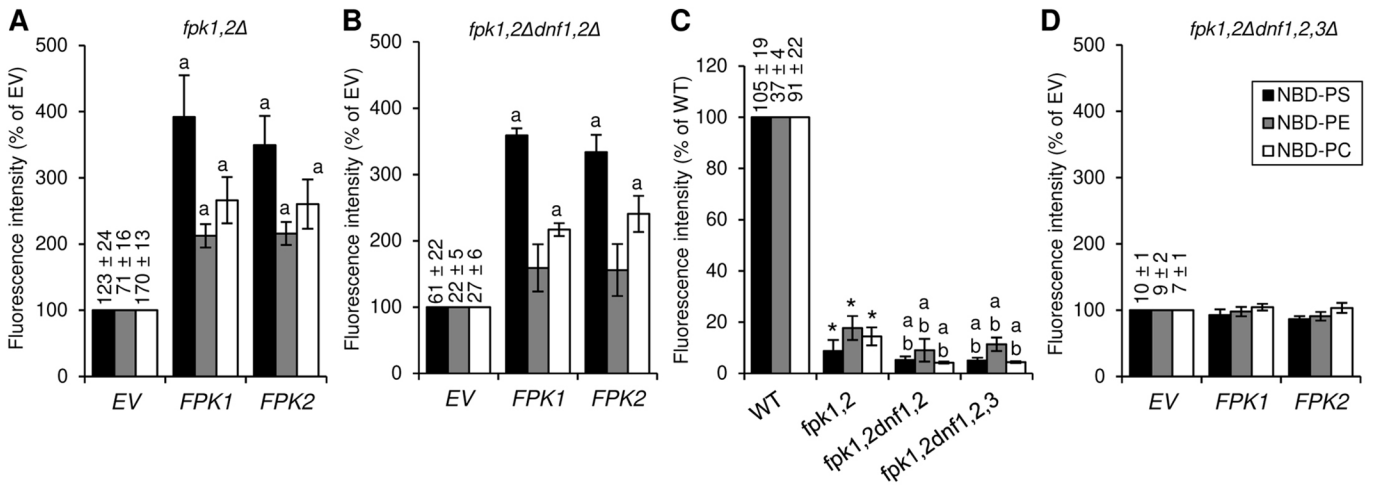

Fig. 2. A phospholipid flippase distinct from Dnf1p and Dnf2p is required for FPK-induced NBD-lipid transport. NBD-lipid uptake by *fpk1,2Δ* cells (A), *fpk1,2Δdnf1,2Δ* (B), and *fpk1,2Δdnf1,2,3Δ* (D) transformed with either an empty vector (EV) or expression plasmids carrying *FPK1* or *FPK2*. (C) Comparison of NBD-lipid uptake between the deletion strains and wild-type KKT61 cells (WT). Accumulation of NBD-lipids is shown as percentage of fluorescence intensity relative to the indicated control cells. Numbers above the bars represent geometric mean±s.e.m fluorescence values. from at least three independent experiments in arbitrary units. *, statistically significant (P<0.01) with respect to all other strains; a, statistically significant (P<0.01) with respect to the empty vector control (A,B,D) or the wild-type strain (C); b, statistically significant (P<0.01) with respect to *fpk1,2Δ* (two-way ANOVA followed by Tukey confidence test).

fpk1,2Δdnf1,2Δ cells, internalization of all three lipids, especially NBD–PE and –PC, was further reduced as compared to *fpk1,2Δ* cells. Further removal of *DNF3* did not have a significant effect, suggesting that Dnf3p activity might be controlled by the Fpk kinases. In agreement to this, we did not observe *FPK*-induced changes in the uptake of any NBD-phospholipid in the *quint* strain, in contrast to the results obtained for the quadruple *fpk1,2Δdnf1,2Δ* mutant (cf. Fig. 2B,D). This finding supports the notion that Dnf3p is responsible for the observed PS transport in the *fpk1,2Δdnf1,2Δ* background and that, when present, Fpk1p and/or Fpk2p activate this transport.

Co-expression of Dnf3p and Fpk1p, but not Drs2p and Fpk1p, results in PS transport across the plasma membrane

To confirm that lack of NBD–PS uptake in *quint* was due to lack of Fpk1p- and Fkp2p-dependent Dnf3p activity, we expressed *FPK1* or *FPK2* and *DNF3* either alone or in combination in the *quint* background. Introduction of *DNF3* alone did not result in increased NBD–PS transport, and the same was true for *quint* cells expressing only *FPK1* (Fig. 3A) or *FPK2* (Fig. S2). However, simultaneous expression of *DNF3* and *FPK1* resulted in an ∼3-fold increase in NBD–PS transport compared to that seen with an empty vector control (Fig. 3A).

To confirm that lack of lipid translocation was not due to lack of protein expression or its inability to reach the plasma membrane, we N-terminally tagged Dnf3p and Fpk1p with decahistidine (RGSH10) and glutathione-S-transferase (GST) tags, respectively. Immunoblot analysis of total membrane fractions demonstrated that Dnf3p is expressed at similar levels in *quint* cells regardless of Fpk1p expression (Fig. 3B). Subcellular localization analysis using sucrose density fractionation demonstrated that Dnf3p is capable of reaching the plasma membrane in an Fpk1p-independent manner (cf. Fig. 3C,D).

To test for transport of endogenous PS, we examined cell growth on medium containing papuamide A. Indeed, *quint* mutant cells were unable to survive in the presence of this toxin (Fig. 3E). Co-expression of *DNF3* and *FPK1* resulted in functional complementation of the papuamide A-sensitive phenotype (Fig. 3E). By contrast, expression of each gene individually did not affect yeast growth. This confirms the notion that co-expression of *FPK1* and *DNF3* generates an activity that results in PS transport at the plasma membrane.

The *quint* strain still contains the *DRS2* gene, which encodes a PS transporter of the TGN (Zhou et al., 2013) that, at least *in vitro*, is a substrate of Fpk1p (Nakano et al., 2008). To test the possible involvement of Drs2p in Fpk1p- and Fkp2p-regulated PS transport into *quint*, we overexpressed RGSH10-tagged *DRS2* and GST–*FPK1* in the *quint* strain and measured transport of NBD–PC, –PE, and –PS. Overexpression of Drs2p alone or in combination with Fpk1p or Fpk2p in *quint* cells did not significantly alter the transport of NBD–PS or any other labeled phospholipid tested (Fig. 3A; Fig. S2). Similarly, yeast growth was not affected when cultured on papuamide A-containing plates (Fig. 3E), even when our *DRS2*-expressing construct was capable of complementing the papuamide A-sensitive phenotype of *dnf1,2Δdrs2Δ* and *dnf1,2,3Δdrs2Δ* strains (Fig. 1C,D), indicating that transport of natural PS was also independent of Drs2p overexpression. The N-terminally decahistidine-tagged Drs2p was expressed at the same level independently of Fpk1p expression (Fig. 3B), and was mainly retained in endomembranes in the absence of Fpk1p (Fig. 3C). Notably, while Fpk1p overexpression did not affect the subcellular localization of Dnf3p, the presence of this kinase increased the amount of Drs2p at the plasma membrane, as indicated by sucrose gradient fractionation (Fig. 3C,D). Taken together, these results suggest that Fpk1p is not capable of activating Drs2p *in vivo*, at least not in the absence of Dnf3p.

Catalytically active Dnf3p and Fpk1p are required for PS transport

To verify that catalytically active Dnf3p and Fpk1p are required for PS transport in the *quint* mutant, we employed the *dnf3E342Q* mutant described above and generated an inactive version of the kinase, *fpk1K525R,* which lacks a conserved lysine residue in the phosphotransfer site (Hanks et al., 1988; Nakano et al., 2008). We expressed combinations of active and inactive versions of Dnf3p and Fpk1p in the *quint* strain and assayed the effect on phospholipid transport and papuamide A sensitivity. NBD–PS transport was only

Journal of Cell Science (2020) 133, jcs235994. doi:10.1242/jcs.235994

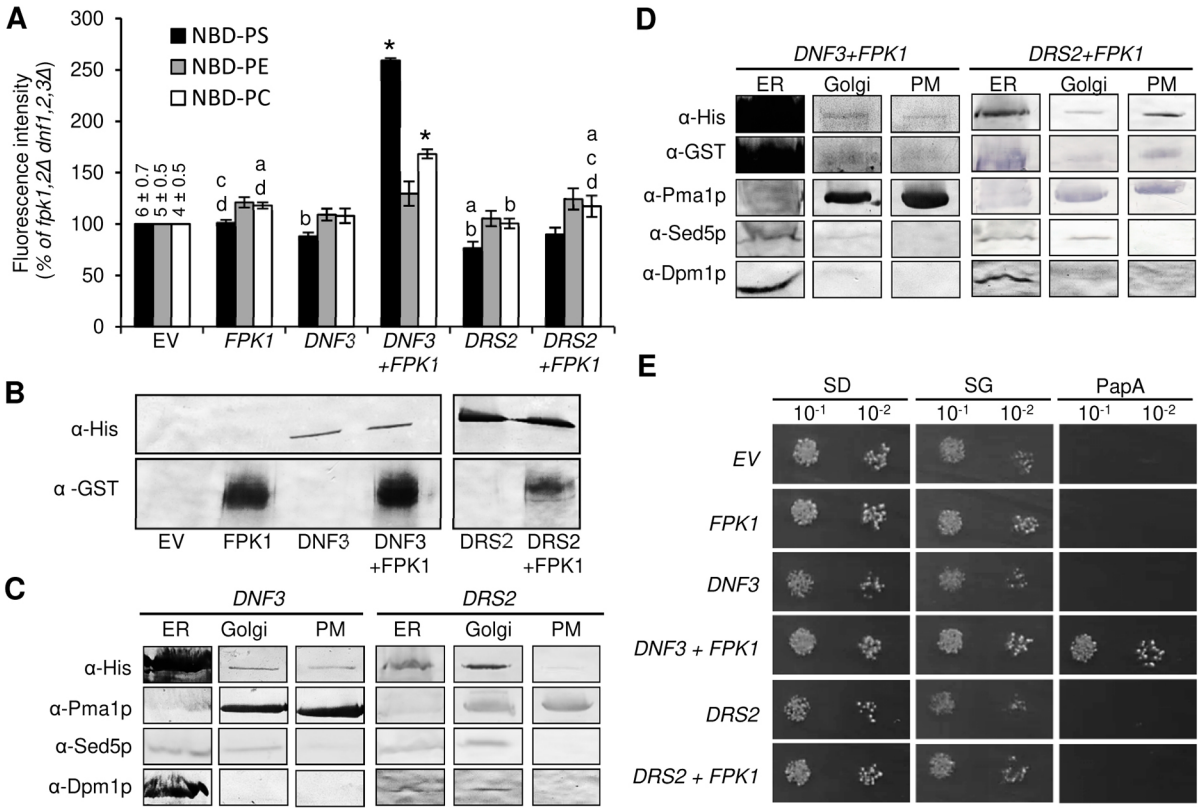

Fig. 3. Overexpression of DNF3 and FPK1, but not DRS2 and FPK1, results in PS transport at the plasma membrane. *fpk1,2Δdnf1,2,3Δ* cells transformed with either empty vector (EV) or expression plasmids carrying *DNF3* or *DRS2* alone or in combination with *FPK1* were analyzed for (A) NBD-lipid uptake, (B) expression of RGSH10-tagged P4 ATPases and GST-tagged Fpk1p in total membrane fractions, (C,D) subcellular localization of the P4 ATPase on sucrose density gradients, and (E) functional complementation of the papuamide A (PapA)-sensitive growth defect. Data in A are shown as percentage of fluorescence intensity relative to empty-vector control cells and represent the mean±s.e.m. from at least three independent experiments. Numbers above the bars represent geometric mean±s.e.m. fluorescence values in arbitrary units. Only differences with respect to the control or to cells expressing *FPK1*, *DNF3* or *DRS2* are included. *, statistically significant (P<0.01) with respect to all other strains; a, statistically significant (P<0.01) with respect to the wild type; b, statistically significant (P<0.01) with respect to cells expressing *FPK1;* c, statistically significant (P<0.01) with respect to cells expressing *DNF3*; d, statistically significant (P<0.01) with respect to cells expressing *DRS2* (two-way ANOVA followed by Tukey confidence test). B–D show immunoblots using antibodies against RGSH10 (α-His) or GST tags or against yeast proteins used as markers for the plasma membrane (α-Pma1p), the Golgi (α-Sed5p), or the endoplasmic reticulum (α-Dpm1p). Cells in E were spotted in two serial dilutions on glucose- (SD, control) or galactose-containing (SG, Induced Expression) plates with no peptide addition or supplemented with PapA as indicated.

detected in cells expressing active versions of both proteins (Fig. 4A). Similarly, inactive mutants did not complement the papuamide A-sensitive growth defect of the *quint* strain (Fig. 4B). All protein variants were expressed at similar levels as detected by immunoblotting (Fig. 4C). We noted that the *fpk1K525R* mutant protein migrated faster in SDS-PAGE gels than did active Fpk1p, probably due to lack of autophosphorylation (Roelants et al., 2010).

Fpk1p has previously been shown to phosphorylate Dnf3p *in vitro* (Nakano et al., 2008). To verify that Fpk1p is an *in vivo* activator of Dnf3p, we employed a previously devised strategy, in which Dnf3p and its β-subunit, Crf1p, are both overexpressed (Nakano et al., 2008). The rationale behind this approach is that overexpression of Dnf3p and Fpk1p, but not Crf1p, results in a relatively small number of catalytically competent Dnf3p–Crf1p complexes that can become highly activated by Fpk1p, whereas overexpression of Dnf3p together with Crf1p produces a large number of catalytically competent complexes with a lower activity that impact phospholipid transport even in the absence of Fpk1p. Therefore, we expressed Dnf3p and Crf1p in the *quint* strain under the control of a strong inducible galactose promoter (Fig. S3). Overexpression of Crf1p and Dnf3p in the absence of Fpk1p complemented the papuamide A-sensitive phenotype of *quint*, confirming that Fpk1p acts upstream of Dnf3p.

Dnf1p, Dnf2p and Dnf3p are involved in morphogenesis during pseudohyphal growth

Under conditions of nitrogen or glucose starvation, diploid *S. cerevisiae* cells switch from the so-called yeast form, characterized by independent budding cells, to a pseudohyphal form, in which cells present an elongated shape and cell division is incomplete, generating short multicellular filamentous structures (Ceccato-antonini and Sudbery, 2004; Karunanithi and Cullen, 2012; Song and Kumar, 2012). These pseudophyphae actively penetrate the growth medium, allowing the cells to scavenge for nutrients that are then delivered to all cells along the filament. In some filamentous fungi, the equivalent process of formation of hyphal structures requires the action of lipid flippases related to yeast Dnf1p and Dnf2p, which are suggested to be involved in lipid redistribution at the point of polarized growth (Schultzhaus et al., 2015). In addition, a relative of Dnf3p in the pathogenic fungi *Magnaporthe grisea* has been shown to be necessary for formation of specialized polarized structures at the tip of penetration hyphae (Balhadère and Talbot, 2001). Based on their common regulation by FPKs, we wondered whether Dnf3p served a role in formation and development of the pseudohyphae in *S. cerevisiae*, in a manner coordinated with Dnf1p and Dfn2p. To investigate this, we

Journal of Cell Science (2020) 133, jcs235994. doi:10.1242/jcs.235994

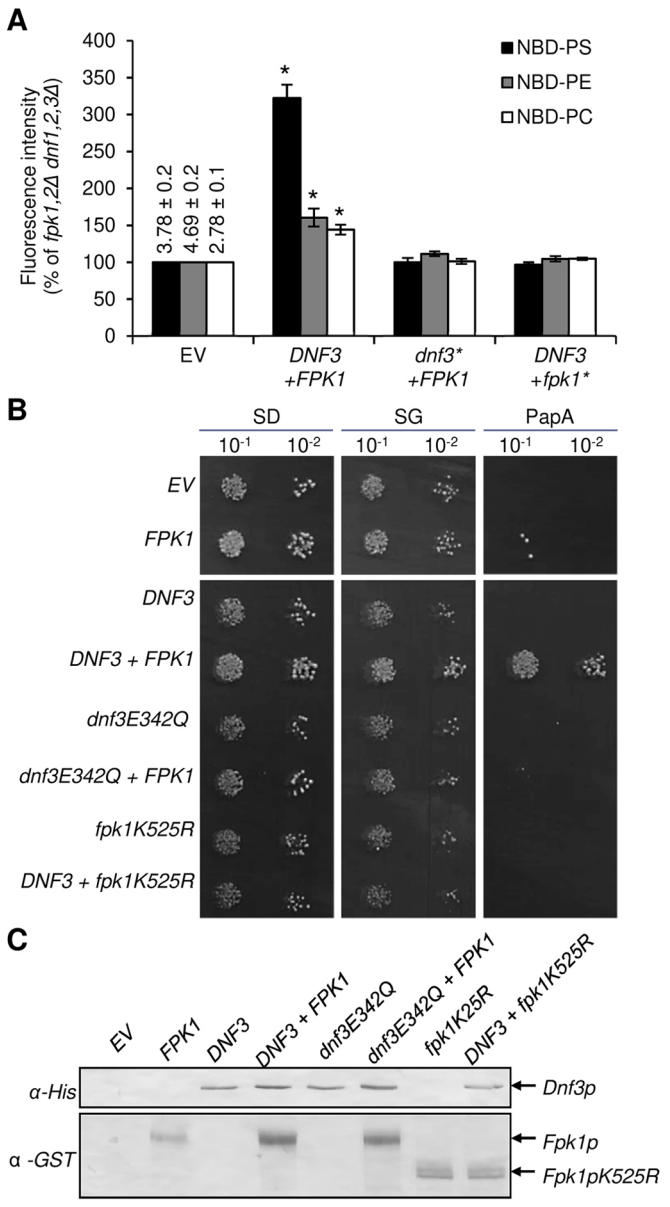

Fig. 4. Catalytically active Dnf3p and Fpk1p are required for PS transport. *fpk1,2Δdnf1,2,3Δ* (*quint*) cells transformed with either empty vector (EV) or expression plasmids carrying active and inactive versions of *DNF3* (*DNF3* and *dnf3E342Q*) and *FPK1* (*FPK1* and *fpk1K525R*) either alone or combined were analyzed for (A) NBD-lipid uptake, (B) functional complementation of the papuamide A (PapA)-sensitive growth defect, and (C) expression of RGSH10-tagged P4-ATPases and GST-tagged Fpk1p probed by immunoblotting. Data in A are shown as the percentage of fluorescence intensity relative to empty vector control cells and represent the means±s.e.m. from at least three independent experiments. Numbers above the bars represent mean±s.e.m. fluorescence values in arbitrary units. $P<0.01$ with respect to all other strains (two-way ANOVA followed by Tukey confidence test). In B, two serial cell dilutions were spotted onto glucose- (SD) or galactose-containing (SG, induced expression) plates, supplemented with PapA as indicated. Numbers indicate cell dilution.

generated single and double mutants of *DNF* genes in a diploid yeast strain, and grew them on solid media lacking nitrogen or glucose to trigger pseudohyphal growth. For quantification, and considering that pseudophyphae formation is a balance between cell elongation and cell division, we defined several parameters that characterize the process: (1) the average pseudohyphal colony size (based on the number of cells forming the colony; Fig. 5A); (2) the proportion of pseudohyphal colonies containing a certain number of cells (e.g. between 20 and 30 cells); (3) the average number of cells per pseudohyphal filament in the colony; and (4) the presence of cells with an elongated shape.

While diploid yeast cells showed a small tendency to form pseudohypal colonies even when grown under control conditions, strains lacking DNF flippases did not show any significant differences with respect to the wild type for any of the tested parameters (Fig. S4). After 12 h of starvation, strains lacking *DNF2* showed an increased colony size in comparison to the wild type or a *dnf1*Δ mutant (Fig. 5B). Interestingly, while deletion of *DNF1* or *DNF3* in the *dnf2*Δ background did not generate any additional effect, an increased colony size was also observed for the *dnf1,3*Δ strain, suggesting that Dnf1p and Dnf3p might have overlapping functions that are similar to those of Dnf2p. In line with this notion, the effect on colony size was exacerbated in the triple *dnf1,2,3*Δ mutant. Analysis of the colony size distribution revealed that a *dnf2,3*Δ mutant accumulated large colonies (>30 cells), while *dnf1,3*Δ accumulated colonies containing 20 to 30 cells. Simultaneous deletion of *DNF1* and *DNF2* also resulted in a higher proportion of large colonies, especially those containing more than 40 cells. This effect was exacerbated in a triple mutant lacking all *DNF* genes, suggesting that coordinated action of all three flippases is required for control of the cell division rate during pseudohyphal growth. Despite the enlarged colony size, the average number of cells per pseudohyphal filament in a colony did not change with respect to the wild type for any of the tested mutants (Fig. 5D), indicating that cell budding was not compromised. After 12 h of starvation, some wild-type cells showed the presence of elongated buds (Fig. 5E). This effect was even more pronounced for *dnf2Δ* cells and exacerbated by deletion of *DNF1*. Further deletion of *DNF3* did not result in any additional effect. These results suggest that Dnf1p and Dnf2p, but not Dnf3p, are required for the control of cell elongation during pseudohyphae development. The involvement of Dnf1p and Dnf2p in cell elongation has been previously demonstrated in haploid cells (Saito et al., 2007). Interestingly, diploid cells grown in control medium containing all nutrients showed a very small proportion of elongated cells that was not significantly affected by deletion of *DNF* genes (Fig. S4).

To further characterize the observed phenotypes, we spotted wild-type and *dnf* diploid mutant cells on plates lacking either nitrogen or glucose and observed the growth after a 12-day incubation (Fig. 6). On these plates, lack of nutrients forces the yeast to penetrate the medium through the formation of pseudohyphae. In order to extend the penetration area, cells divide and expand laterally, generating an outer ring of cells, whose size can be easily measured after microscopic visualization. Deletion of different *DNF* combinations did not cause any significant effects on outer ring expansion under nitrogen-starvation conditions (Fig. 6A,C, unwashed). On glucose-depleted medium, where cells are subjected to an additional metabolic stress, deletion of *DNF1* caused an increase in the size of the outer ring, while deletion of *DNF2* resulted in a reduced size (Fig. 6B,D, unwashed). A double *dnf1,2Δ* mutant showed a reduction of the outer ring size in addition to that for *dnf2Δ*, suggesting that *DNF1* and *DNF2* have complementary functions in outer ring expansion and that the increased ring size observed for *dnf1Δ* might be due to a compensatory effect of Dnf2p or Dnf3p activity in the absence of *DNF1*. Interestingly, a double *dnf2,3Δ* mutant did not show any significant differences with respect to the wild type, suggesting

Journal of Cell Science (2020) 133, jcs235994. doi:10.1242/jcs.235994

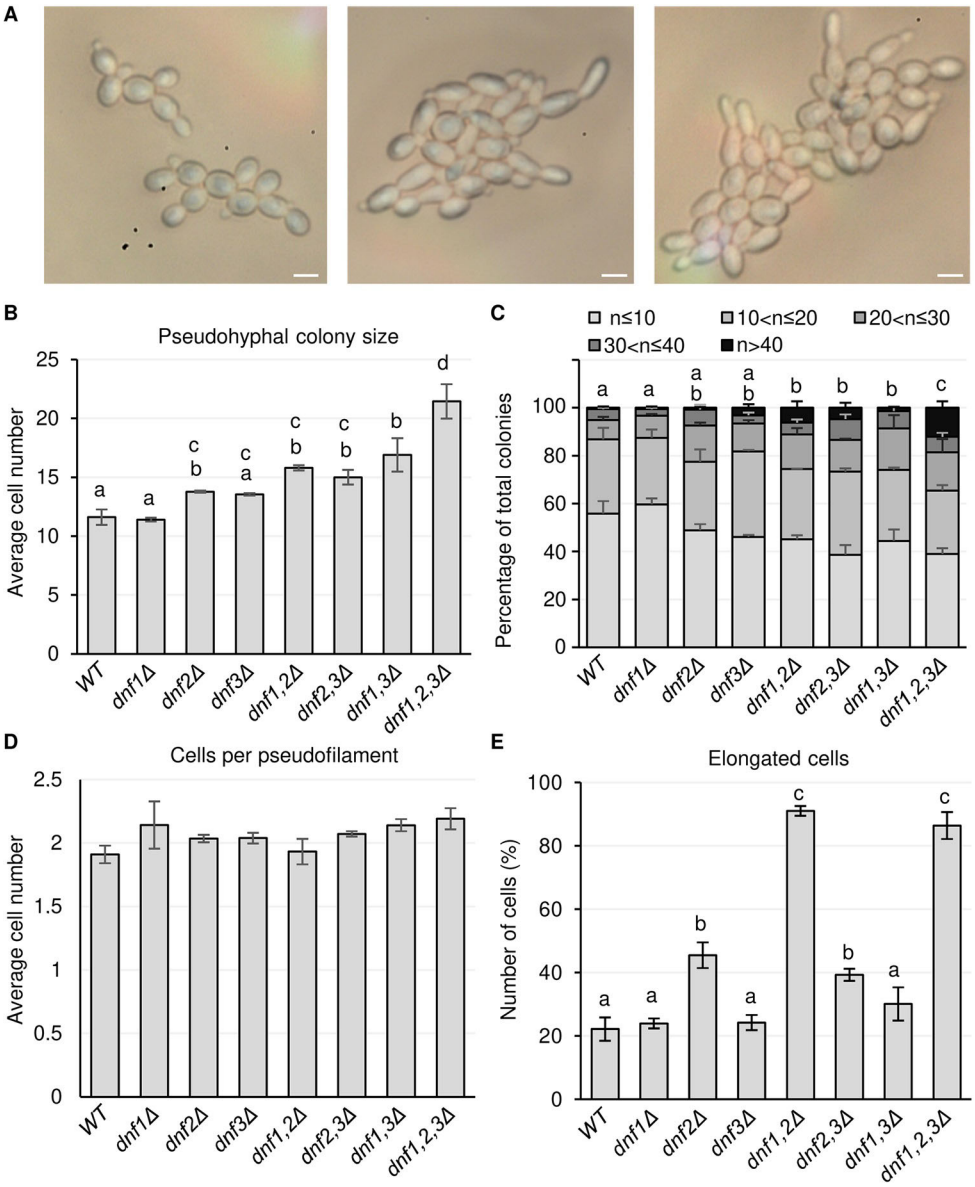

Fig. 5. Deletion of *DNF* genes results in yeast mutants with defects in cell elongation and pseudohyphal growth. Yeast wild-type and *dnf* knockout cells were spotted onto plates without nitrogen and observed under the microscope after 12 h. (A) Representative images for at least 100 wild-type pseudohyphal colonies with <20 cells (left), between 20 and 40 cells (middle) or >40 cells (right). Scale bars: 10 µm. (B–D) Pseudohyphal colony growth was characterized by the average number of cells forming the colony (B), the proportion of colonies with a specific number (*n*) of cells (C), and the average number of cells per pseudohyphal filament in a colony (D). The number of elongated cells in the culture was also quantified for each yeast strain (E). Results are mean ±s.e.m. from at least three independent experiments, in which at least 900 cells per strain were counted. Values not sharing a common superscript letter differ significantly at $P<0.01$ according to a multinomial analysis (C) or a two-way ANOVA followed by Tukey confidence test (B,D,E). See Materials and Methods for details.

that either Dnf2p and Dnf3p have opposite functions in outer ring expansion, or that Dnf1p activity is increased to compensate for absence of *DNF3* in the double *dnf2,3Δ* mutant. The changes in outer ring size seemed to be concomitant with a change in the penetrating capacity of the pseudohyphae, which can be observed after removal of surface cells by washing (Fig. 6, washed). In this case, a statistically significant reduction of the outer ring size was observed for *dnf1,2,3Δ* with respect to a double *dnf1,2Δ* mutant under all nutritional conditions tested, suggesting *DNF3* might be partly compensating for loss of *DNF1* function in *dnf1,2Δ*.

In addition to the changes in outer ring size, pseudohyphal colonies lacking DNF proteins showed several morphological defects (Fig. 6A,B; Fig. S5). While single *dnf1Δ* and double *dnf1,3Δ* mutants showed more or less circular colonies with a homogenous perimeter, removal of *DNF2* resulted in the formation of pseudohyphae that project out of the colony generating an uneven perimeter. This effect was exacerbated in *dnf2,3Δ*, but not in a *dnf1,2Δ*, mutant, while it seemed to be reduced in *dnf1,2,3Δ*. However, the morphological defects in *dnf1,2,3Δ* might be masked by the heavily reduced size of the outer ring. Interestingly, *dnf3Δ* showed a similar, albeit less pronounced, phenotype to *dnf2Δ* with respect to the circularity of the colony (Fig. 6; Fig. S5). In addition, single deletion of *DNF3* resulted in the formation of drop-like structures on the surface of the colony. Taken together, these results suggest that *DNF2* and *DNF3* are important for uniform pseudohyphal expansion.

Dnf3p appeared at the origin of fungal evolution

Previous phylogenomic analysis of P4 ATPase sequences from fungi, animals and plants revealed that Dnf3p is related to a group of fungal sequences with no obvious relationship to any other P4 ATPases (Palmgren et al., 2019; Poulsen et al., 2015). Thus, having identified Dnf3p as a novel system for flipping PS at the plasma membrane in *S. cerevisiae*, we wondered how this system had evolved in fungi. For this purpose, we first selected 37 fungi from all major fungal lineages, identified all P4 ATPases in their genomes and subjected them to a phylogenetic analysis (Fig. 7). Two subfamilies of P4 ATPases, P4A and P4B could be identified, as previously described (Palmgren et al., 2019). Fungal P4B ATPases

Journal of Cell Science (2020) 133, jcs235994. doi:10.1242/jcs.235994

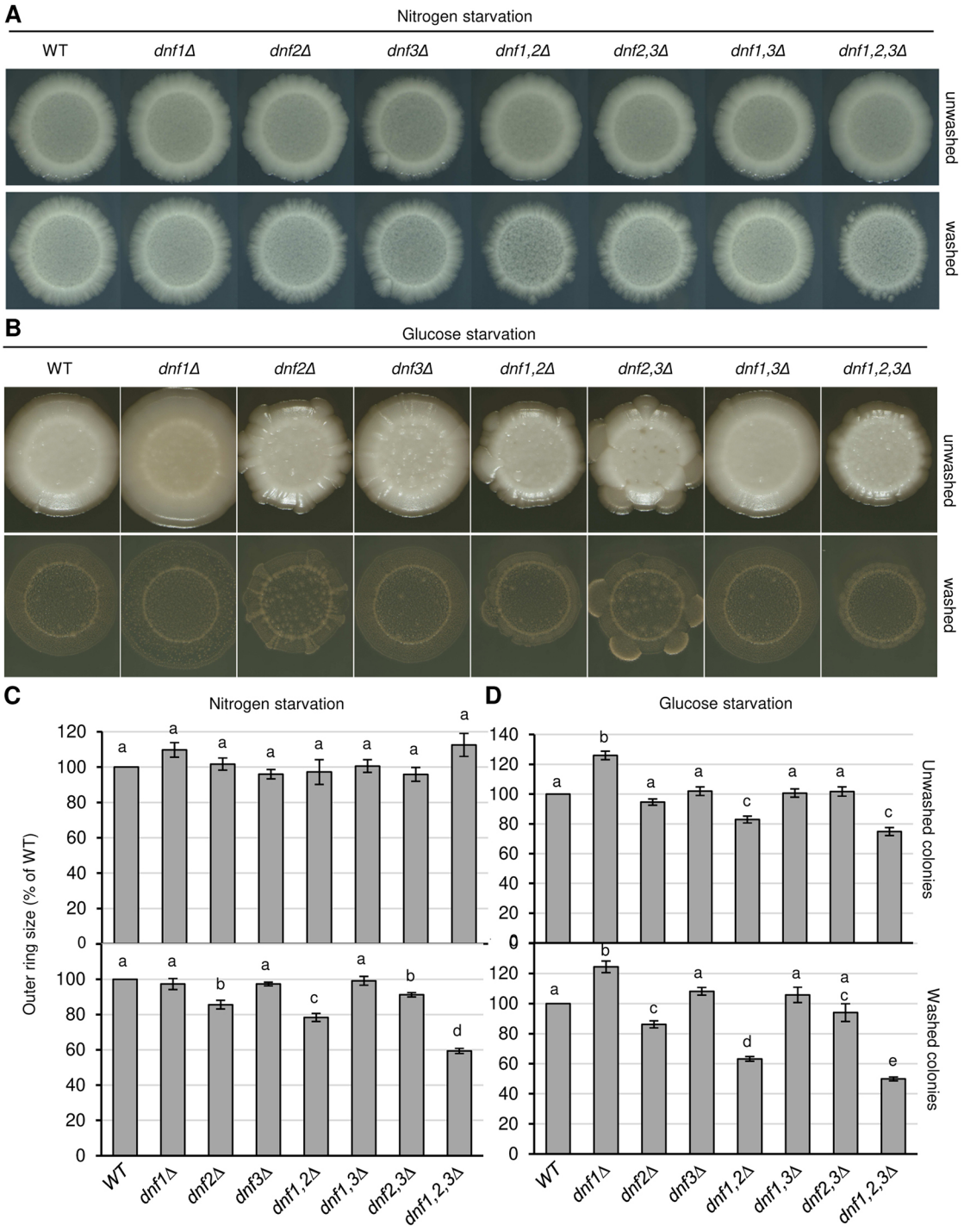

Fig. 6. Yeast strains lacking DNF proteins show morphological defects in pseudohyphal expansion that are concomitant with changes in the invasive growth profile. Yeast wild-type and *DNF* knockout cells were spotted onto plates (A) without nitrogen or (B) without glucose. Plates were observed at the microscope after a 12-day incubation and images were taken before and after wash with water to study colony morphology and pseudophyphae invasiveness, respectively. (C,D) The average size of the outer ring was measured for each colony as described in the Materials and Methods and normalized to wild-type values. Results are mean±s.e.m. from at least three independent experiments, in which at least 900 cells per strain were counted. Values not sharing a common superscript letter differ significantly at $P<0.01$ according to a two-way ANOVA followed by Tukey confidence test.

comprised a single monophyletic clade represented in *S. cerevisiae* by Neo1p, and all fungal genomes analyzed included at least one gene belonging to this clade. Fungal P4A ATPases could further be divided into four clades. A minor basal clade only had members from early diverging lineages of fungi, whereas three remaining clades each had a *S. cerevisiae* representative (designated the Drs2p, Dnf1p/2p, and Dnf3p clades, respectively). The Dnf1p/2p clade showed signs of an early gene duplication and subsequent gene loss of one of the copies in Ascomycota (Fig. 7). A Dnf3p homolog could be found in all fungal genomes except in those from Basidiomycota (Fig. 7A). Taken together, Dnf3p-like sequences are present in the earliest fungi but have been subsequently lost in

Journal of Cell Science

Journal of Cell Science (2020) 133, jcs235994. doi:10.1242/jcs.235994

Basidiomycota, which, on the other hand, have retained both copies of an early Dnf1p/2p ATPase duplication, among which one was lost in Ascomycota.

To determine whether Dnf3p-like sequences are specific for the fungal kingdom, we searched for homologs among all P4 ATPase sequences extracted from the Kyoto Encyclopedia of Genes and Genomes (KEGG) collection of organisms with complete genomes. We then expanded the phylogenetic analysis to include the fungal sequences identified above and, in addition, identified the 100 sequences with highest similarity to Dnf3p that resulted from a BLAST search in the National Center for Biotechnology Information (NCBI) protein database, both when 'Fungi' were excluded from the search and when 'Fungi' were searched excluding Basidiomycota. The resulting tree (Fig. 8) included the Dnf3p clade within P4A ATPases (Palmgren et al., 2019), but this clade did not group with any other clade in the tree. The only exception to fungal sequences in the Dnf3p clade was a sequence (XP_009493813) from *Fonticula alba*, which appeared at the base of the clade. *Fonticula* is an amoeboid genus that has been characterized as the sister group to fungi (Brown et al., 2009; Kiss et al., 2019). A *F. alba* sequence was also found at the base of the fungal Dnf1p/2p clade. Taken together, these results show that the Dnf3p clade is unique for fungi and evolved at the very onset of fungal evolution.

DISCUSSION

In this work, we demonstrate that Dnf3p is a transporter of endogenous PS in both endomembranes and the plasma membrane. Previous work presented evidence that Dnf3p primarily transports PC and PE (Alder-Baerens et al., 2006). This conclusion was based on studies of late post-Golgi vesicles purified from a yeast strain lacking *DRS2* and carrying the *sec6-4* mutation (Alder-Baerens et al., 2006; Lamping et al., 2005). As this strain still expresses Dnf1p and Dnf2p, which are known to primarily transport PC and PE (Pomorski et al., 2003), it is possible that the measured fluorescent lipid uptake might partially have been caused by the activity of Dnf1p and Dnf2p, which may explain the discrepancy with the results reported here. In support of this, the amount of Dnf3p in metabolically active yeast cells is ∼40 times lower than that of Dnf1p and 15 times lower than that of Dnf2p (Hua et al., 2002). Moreover, Dnf1p and Dnf2p are required for proper sorting of tryptophan permease Tat2p at the TGN, which suggests these flippases are active in endomembranes (Hachiro et al., 2013).

One prominent example of polarized growth in yeast cells is pseudohyphal growth. Our phenotypic analysis of yeast mutants lacking different combinations of the Dnf proteins indicates that Dnf3p is involved in control of lateral expansion during pseudophyphal growth, and that its physiological function is coordinated with that of Dnf1p and Dnf2p during this process. In addition, Dnf3p is also involved, together with Dnf2p, in controlling homogenous pseudohyphal expansion. The Dnf3p homolog PDE1 from the pathogenic fungi *Magnaporthe grisea* plays an essential function in host-cell penetration, a process that, similar to mating tip (schmoo) formation in yeast, requires polarized growth (Balhadère and Talbot, 2001). This would suggest that homologs of Dnf3p in other fungi also contribute to polarized growth.

Owing to its physiological relevance, P4 ATPase activity must be tightly regulated. Drs2p is regulated by interaction with lipids and proteins involved in the process of vesicle formation in the secretory pathway (Azouaoui et al., 2017; Chantalat et al., 2004; Natarajan et al., 2009; Tsai et al., 2013). The two yeast plasma membrane P4 ATPases, Dnf1p and Dnf2p, are activated by specific kinases named flippase kinase (Fpk) 1 and 2 (Nakano et al., 2008). In turn, an upstream kinase cascade controls the activity of Fpk1p and Fpk2p (Roelants et al., 2010, 2015; Sartorel et al., 2015), suggesting a coordinated regulation of flippases by cellular responses. It was previously shown that the kinase domain of Fpk1p, which is required for Dnf1p and Dnf2p activation, can phosphorylate Dnf3p *in vitro* (Nakano et al., 2008). In the present work, we expressed a full-length version of Fpk1p and demonstrated that this kinase is required for Dnf3p activity *in vivo*. In support of this, inactivating mutations in *DNF3* rescue the growth ability of yeast mutants carrying temperature-sensitive versions of Ypk1p and Ypk2p (Roelants et al., 2002), two kinases that form part of a three-tiered kinase cascade that also involves Fpk1p and Fpk2p (Roelants et al., 2010).

Our findings that Fpk1p activates Dnf3p and that Dnf3p reaches the plasma membrane in a cell cycle-dependent manner have further implications for our understanding of the role of flippase kinases in the control of the yeast cell cycle. During progression through the cell cycle, the protein kinase Gin4p localizes at the incipient bud site, and phosphorylates and inhibits Fpk1p at the same location, which in turn increases the activity of Cdc42p (Roelants et al., 2015). Cdc42p is a small GTPase required for the recruitment and function of effectors that promote bud emergence (Atkins et al., 2013; Lo et al., 2013; Saito et al., 2007; Tong et al., 2007). As recruitment of Cdc42p to the plasma membrane depends on PS internalization (Fairn et al., 2011), our results suggest that Gin4p might exert at least parts of its effect indirectly via inhibition of Dnf3p.

The existence of a common regulatory mechanism for all Dnf proteins also has consequences for our understanding of the formation of the shmoo, another example of cell polarity in *S. cerevisiae*. Shortly after exposure to α-mating factor, Dnf1p, Dnf2p, Dnf3p and Fpk1 are all localized to the mating tip, and a *dnf1Δdnf2Δdnf3Δ* mutant has a defect in mating (Sartorel et al., 2015) that is equivalent to that of a *fpk1Δfpk2Δ* mutant. This defect relates to instability of Ste5p, a scaffold protein that is normally recruited to the shmoo tip for initiation of α-factor signaling (Pryciak and Huntress, 1998), and mislocalization of Mss4p, a plasma membrane phosphatidylinositol-4-phosphate 5-kinase that has been implicated in the establishment of cell polarity (Orlando et al., 2008; Yakir-Tamang and Gerst, 2009). Although these deficiencies were linked to loss of PS internalization, no evidence was presented for the specific involvement of Dnf1p, Dnf2p or Dnf3p in this process (Sartorel et al., 2015). In light of the results reported here, it is likely that it is Dnf3p that internalizes PS at the shmoo and is hence responsible for recruitment of Ste5p and Mss4p.

Our results indicate that Dnf3p is a PS transporter that evolved to complement a flippase kinase-controlled system at the plasma membrane that also includes Dnf1p and Dnf2p. The emergence of a system that created PS asymmetry in the plasma membrane may have been a crucial early event in fungal evolution that coincided with the appearance of polarized growth processes such as substrate penetration and the formation of hyphae. Notably, Dnf3p-like sequences are absent from Basidiomycota, which instead, with no exceptions, harbored representatives of a subclade in the Dnf1p/2p clade not present in Ascomycota, but shared with primitive fungal groups. This raises the question of whether sequences in this subclade replaced Dnf3p to carry out a similar function in polar growth in Basidiomycota.

Our phylogenetic analyses of P4 ATPase sequences demonstrate that the ancestor of the Dnf3p subclass of P4 ATPases emerged at the very base of the fungal tree. Their presence in *Fonticula*, a sister group

Journal of Cell Science (2020) 133, jcs235994. doi:10.1242/jcs.235994

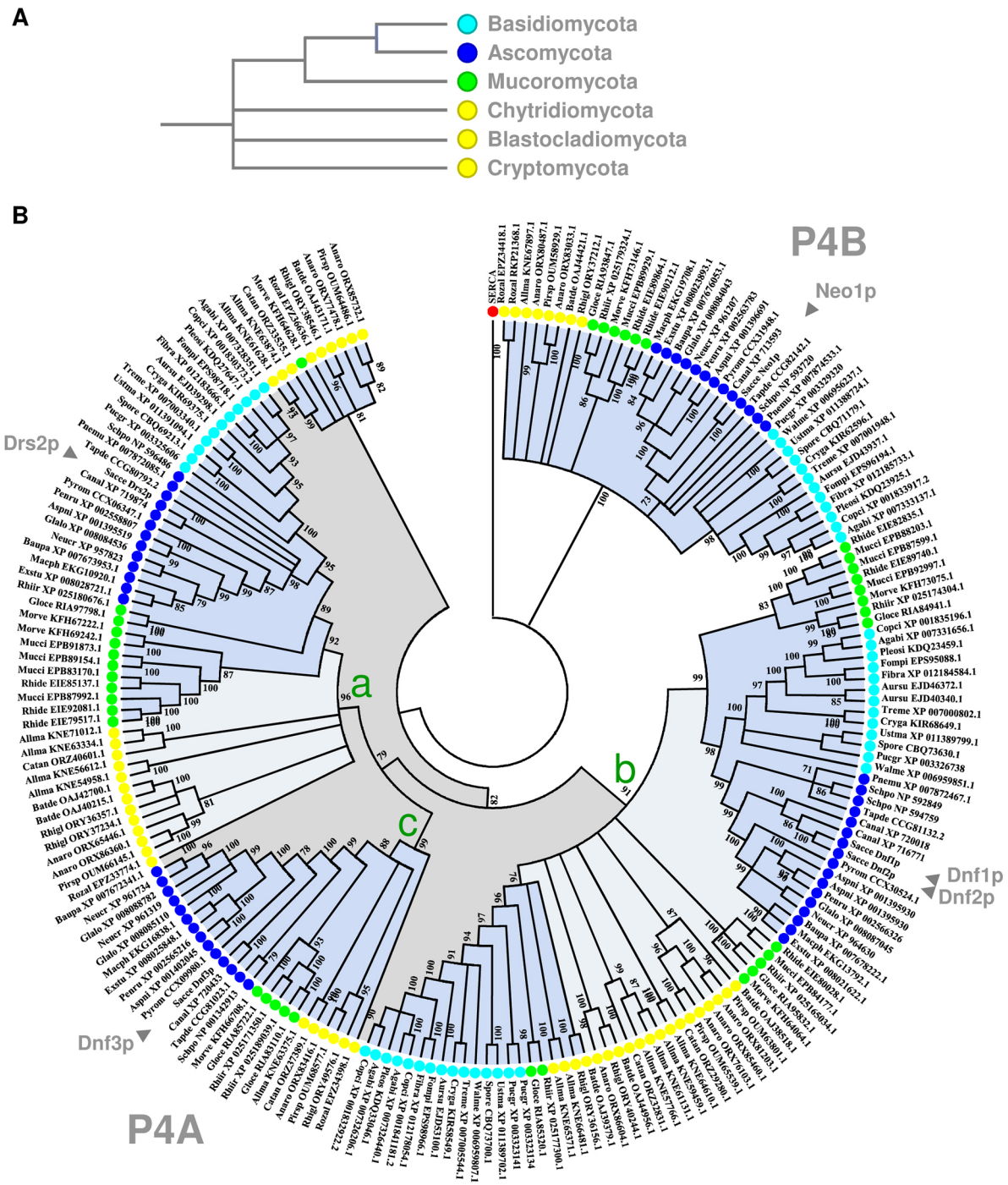

Fig. 7. Five clades of P4 pumps are present in fungi. (A) Schematic of the relationship between fungal phylae represented in B. (B) Phylogenetic tree of 202 sequences representing all P4 ATPases from 37 fungal species and a rabbit (*Oryctolagus cuniculus*) SERCA pump protein sequence as outgroup. The fungal species represent the major phylae of the fungal kingdom. The phylogenetic tree was inferred from maximum likelihood analysis with 1000 bootstrap iterations, performed using the RAxML program version 8.2.1. Node values represent maximum likelihood statistical values with a maximum of 100%. All nodes with statistical values less than 60% were collapsed into multifurcations and only values of 75% or above are shown. In the phylogenetic tree, proteins belonging to the P4A clade are outlined in light gray, with individual groups in light blue. The P4B clade is outlined in blue. Proteins are preceded by a colored circle representing the corresponding phylum of the species. The species are as follows. Light blue: Basidiomycota: Aursu, *Auricularia subglabra*; Fompi, *Fomitopsis pinicola*; Fibra, *Fibroporia radiculosa*; Pleos, *Pleurotus ostreatus*; Copci, *Coprinopsis cinerea*; Cryga, *Cryptococcus gattii*; Treme, *Tremella mesenterica*; Pucgr, *Puccinia graminis*; Spore, *Sporisorium reilianum*; Ustma, *Ustilago maydis*; Walme, *Wallemia mellicola*. Dark blue: Ascomycota: Pyrom, *Pyronema omphalodes*; Macph, *Macrophomina phaseolina*; Baupa, *Baudoinia panamericana*; Exstu, *Exserohilum turcica*; Aspni, *Aspergillus niger*; Penru, *Penicillium rubens*; Glalo, *Glarea lozoyensis*; Neucr, *Neurospora crassa*; Canal, *Candida albicans*; Sacce, *Saccharomyces cerevisiae*; Pnemu, *Pneumocystis murina*; Schpo, *Schizosaccharomyces pombe*; Tapde, *Taphrina deformans*. Green: Mucoromycota: Gloce, *Glomus cerebriforme*, Rhiir, *Rhizophagus irregularis*; Morve, *Mortierella verticillata*; Mucci, Mucor *circinelloides*; Rhide, *Rhizopus delemar*. Yellow: Blastocladiomycota: *Allomyces macrogynus*; Catan, *Catenaria anguillulae*. Chytridiomycota: Rhigl, *Rhizoclosmatium globosum*; Batde, *Batrachochytrium dendrobatidis*; Anaro, *Anaeromyces robustus*; Pirsp, *Piromyces sp.* Cryptomycota: Rozal, *Rozella allomycis.*

Journal of Cell Science (2020) 133, jcs235994. doi:10.1242/jcs.235994

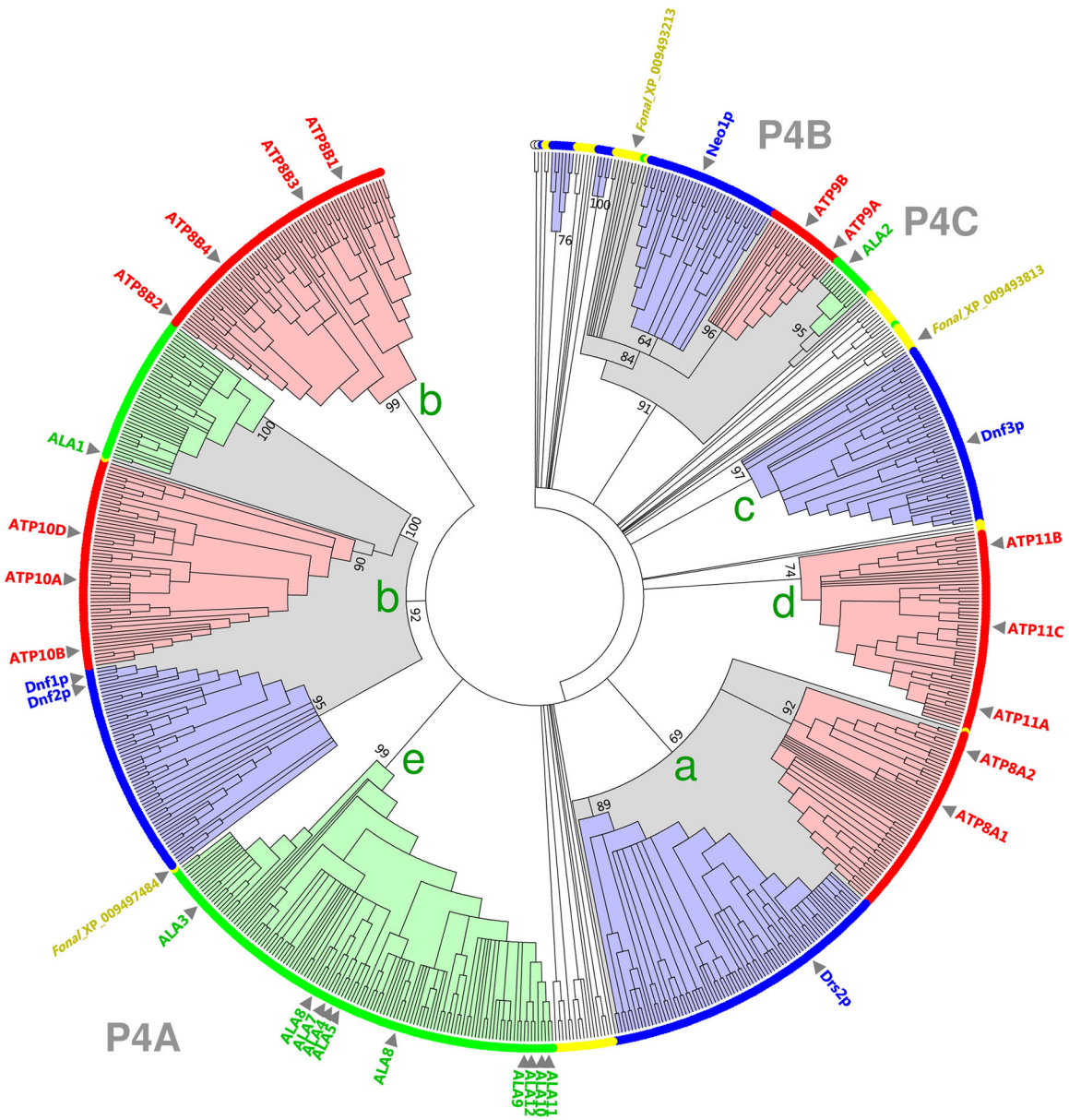

Fig. 8. The Dnf3p group of P4 ATPases is specific for fungi. A phylogenetic tree is shown that was inferred from maximum likelihood analysis of 751 P4 ATPase sequences from various eukaryotic super groups collected as described in the Materials and Methods. P5 ATPases *A. thaliana* MIA and *H. sapiens* ATP13A1 were used as the outgroups. In the phylogenetic tree, sequences are labeled with a colored circle representing to which eukaryotic super group they belong: *blue*, fungi; *red*, animals; *green*, Viridiplantae; *yellow*, other eukaryotic super groups ('protists'). Clades are colored according to the same color code. Clades that are united with a bootstrap value of more than 60% and may have a common origin are marked with gray background color. Arrowheads with sequence names mark the position of *S. cerevisiae*, *A. thaliana*, *H. sapiens* and *F. alba* sequences (in the latter case only sequences belonging to the major fungal clades are marked). The phylogenetic tree was inferred from a maximum likelihood analysis with 1000 bootstrap iterations. Node values represent maximum likelihood statistical values with a maximum of 100%. All nodes with statistical values less than 60% were collapsed into multifurcations and only values of 60% or above are shown.

to true Fungi, is noteworthy. *Fonticula* morphologically resembles slime molds and do not develop hyphae. It may be that *Fonticula* has evolved an as yet uncharacterized mechanism for polarized growth that, in true fungi, became a basis for hyphal growth. This would suggest that the emergence of Dnf3p to complement the work of Dnf1p and Dnf2p represents a hallmark of fungal evolution.

To conclude, we present evidence that Dnf3p is able to transport PS, in addition to PC and PE, and is subject to regulation by Fpk kinases that control Dnf1/2p activity. Through phenotypic analysis we demonstrate that the action of Dnf1p, Dnf2p and Dnf3p is required for pseudohyphal growth. This, together with the results of our phylogenetic analyses and the physiological evidence gathered from filamentous fungi, suggests that Dnf1p, Dnf2p and Dnf3p play important roles in regulating polarized growth.

MATERIALS AND METHODS

All chemicals were purchased from Sigma-Aldrich, St Louis, MO, USA, unless otherwise stated.

Yeast strains

Yeast strains used in this study are listed in Table S1. *DNF1*, *DNF2* and *DNF3* were sequentially removed in an *fpk1,2Δ* strain (Nakano et al., 2008)

kindly provided by Kazuma Tanaka, Hokkaido University, Japan (KKT268), by transforming yeasts with linearized gene-deletion constructs consisting of a loxp:*HIS3*:loxp cassette flanked by 500 base pair (bp)-long recombination sites corresponding to the promoter and terminator regions for the desired gene (Pomorski et al., 2003). *HIS3* was subsequently removed by expression of Cre recombinase from a plasmid (Sauer, 1987). All integration and dis-integration events were verified by yeast colony PCR with Phusion polymerase (Fisher Scientific Fermentas, Waltham, MA) according to manufacturer's instructions using the primers listed in Table S2. For C-terminal tagging of the endogenous copy of *DNF3*, a DNA construct containing the SNAP fragment cloned between the EcoRI and SalI restriction sites of plasmid pRS423-GAL (Burgers, 1999) was generated. This template was then used to amplify a PCR fragment containing the SNAP tag sequence followed by a *HIS3* reporter gene, using primers that generate 30 bp-long homologous regions to the final nucleotides of the *DNF3* open reading frame and the *DNF3* 3′-UTRs, respectively. The PCR product was subsequently transformed into wild-type BY4741 and integration of the fragment was checked by PCR as above. For cell morphology, pseudohyphae formation and invasive growth studies Δ*dnf*1, Δ*dnf2* and/or Δ*dnf*3 single, double and triple knockout yeast in *MAT**a***-Y825 and *MAT**α***-HLY337 backgrounds (Johnson et al., 2014) (a kind gift from Anuj Kumar, University of Michigan) were generated. Gene deletions were carried out by transforming yeast with respective knockout cassettes consisting of the *loxP*::*URA3*::*loxP* cassette with ∼500 base pair recombination sites for the promoter region and 3′-end region of the *DNF* genes. *DNF* gene knockout cassettes were obtained by PCR using oli5338 and oli5339 with pMP5029, pMP5030 and pMP5031 as templates to amplify, respectively, *DNF1*, *DNF2* and *DNF*3 knockout cassettes. A subsequent removal of the *URA3* marker was performed by excisive recombination using Cre recombinase (Sauer, 1987). The generation of double and triple gene deletions were performed sequentially by repeated use of the *loxP::URA3::loxP* cassette and subsequent removal of the *URA3* marker by excisive recombination using Cre recombinase. All integration and dis-integration events were verified by PCR. Diploid strains were then generated by mating the respective knockout haploid strains.

Yeast plasmids and cloning

All plasmids (listed in Table S2) were constructed by PCR amplification using Phusion polymerase (Fisher Scientific Fermentas, Waltham, MA, USA) following manufacturer's instructions. Primers are listed in Table S3. *FPK1* and *FPK2* were amplified from *S. cerevisiae* strain BY4741 genomic DNA. PCR-products were cloned into pENTR™/D-TOPO (Invitrogen, Carlsbad, CA, USA) and subsequently transferred to the Gateway®-compatible destination vector pMP2355, created by inserting Gateway® Reading Frame Casette A in the unique HincII site of pRS425-GAL (Burgers, 1999), using the Gateway® Vector Conversion System (Invitrogen, Carlsbad, CA, USA). This resulted in plasmids pMP3859 (*FKP1*) and pMP3714 (*FPK2*). Full-length *FPK1* was N-terminally tagged by two-step PCR-cloning. First, two overlapping PCR fragments corresponding to GST and FPK1 were amplified from pGEX-4T-1 (GE Healthcare, Amersham, UK) and pMP3859, respectively. A full-length overlapping PCR was then performed using the purified PCR products as templates. The final product was ligated into pENTR™/D-TOPO and transferred to pMP2355 using Gateway® technology (Invitrogen, Carlsbad, CA, USA). *DNF3* was amplified from a plasmid (kindly provided by Joost Holthuis, University Osnabrück, Germany) with primers including EcoRI and SalI restriction sites at the 5′- and 3′-ends, respectively. The resulting PCR-product was ligated into pENTR™/D-TOPO and inserted into the Gateway®-compatible vector pMP1965 (Poulsen et al., 2008) rendering plasmid pMP4077. *DNF3* was transferred to pMP4062 (López-Marqués et al., 2012) by EcoRI/SalI digestion to obtain N-terminally RGSH10-tagged *DNF3* under the control of a *GAL1-10* promoter. The same strategy was used to generate N-terminally RGSH10-tagged *DRS2* by transferring the gene from pMP2340 (López-Marqués et al., 2010) to pMP4062. *DNF1* and *DNF2* were amplified from plasmids (kindly provided by Joost Holthuis) and cloned by homologous recombination into pMP4062 using the ZHY709 yeast strain (Hua et al., 2002) as a host. Site-directed mutagenesis to obtain *dnf3E342Q*, *dnf3D566N* and *fpk1K525R* was performed with the QuikChange XL Gold Mutagenesis Kit (Stratagene, La Jolla, CA, USA), according to manufacturer's instructions and the primers listed in Table S3.

DNF1-, *DNF2*- and *DNF3-URA3* knockout cassettes were generated through a homologous recombination strategy in which the *URA3* fragment was amplified by PCR (Oli5338 and Oli5339 with loxp sequence overhangs) using pRS423-GAL as template (Burgers, 1999), resulting in PCR fragments containing a loxp sequence overlap in the *loxP*:*HIS3*:*loxP* plasmids pMP4967, pMP4968 and pMP4969 (Pomorski et al., 2003). PCR fragments were transformed into yeast strain ZHY709 together with linearized plasmids digested with *BclI*. This resulted in pMP4029, pMP5030 and pMP5031 containing, respectively, *DNF1*-, *DNF2*- and *DNF3-URA3* knockout cassettes.

For cloning of *GFP*-tagged *DRS2* and *DFN3*, *yeGFP* was PCR amplified with primers oli2774 and oli2775 (Table S3). Homologous recombination in yeast of the PCR fragment into *EcoRI*-linearized pMP423-GAL (Burgers, 1999) resulted in plasmid pMP3129. Constructs in pMP4062 (see above) were then used to transfer *DRS2* and *DNF3* into pMP3129 by *EcoRI*/*SalI* digestion.

Yeast transformation and media

All yeast media reagents were purchased from BD Bioscience (Albertslund, Denmark), unless otherwise stated. Yeast transformations were performed by the lithium acetate method (Gietz and Woods, 2002). Cells were grown at 30°C in YPD (1% w/v yeast extract, 2% w/v bacto-peptone, 2% w/v glucose) or in rich synthetic medium containing 0.7% w/v Yeast Nitrogen Base, 1.4 g/l of Yeast Synthetic Drop-out Medium Supplements without the desired amino acids (Sigma-Aldrich), and 2% w/v glucose (SD), galactose (SG) or galactose/fructose (SGF). For cell elongation/pseudohyphae formation and invasive growth studies, medium without a nitrogen (2% w/v glucose, 0.7% w/v yeast nitrogen base without nitrogen, 0.05 mM ammonium sulfate, 0.03 mg/ml leucine, 0.02 mg/ml tryptophan and uracil) or glucose (1% w/v yeast extract and 2% w/v peptone) was used. For solid media, 2% agar was added.

Membrane preparation and protein immunodetection

Total membrane preparations were performed essentially as described previously (Villalba et al., 1992). Fresh yeast transformants were inoculated in selective SD medium and grown for 24 h at 28°C with 100 rpm shaking, before inoculation into SG medium at a 1:100 dilution. After another 24-h incubation period under the same conditions, cells were harvested by centrifugation (3000 ***g***, 4°C, 5 min), washed twice in ice-cold water and resuspended 1/1 (w/v) in homogenization buffer (45% glycerol, 200 mM Tris-HCl pH 7.5, 40 mM EDTA, 0.5 µg/ml pepstatin A, 50 µM phenylmethylsulfonyl fluoride, 0.5 mM dithiothreitol). Cells were lysed by addition of one volume ice-cold acid-washed glass beads (0.5 mm), followed by four cycles of 1 min vortex and 1 min incubation on ice. Samples were diluted to a half with GTED20 (20% glycerol, 100 mM Tris-HCl pH 7.5, 1 mM EDTA, 1 µg/ml pepstatin A, 0.1 mM phenylmethylsulfonyl fluoride, 1 mM dithiothreitol) and centrifuged (3000 ***g***, 4°C, 10 min) to eliminate glass beads and cell debris. Total microsomal membrane fractions were collected by centrifugation at 100,000 ***g*** at 4°C for 1 h and homogenized in GTED20. Protein samples were quantified by the method of Bradford using bovine serum albumin (BSA) as a standard. For protein blot analysis of total membrane fractions, 40 µg total protein were precipitated with trichloroacetic acid.

For sucrose-density fractionation, fresh yeast transformants were inoculated in 50 ml selective SG media and grown for 24 h at 28°C under 160 rpm shaking. Cells were harvested (1500 ***g***, 5 min, 24°C) and inoculated into 500 ml fresh SG medium. Cultures were grown to at optical density at 600 nm (OD_{600}) of 1–1.2 at 28°C under 160 rpm shaking. Cells (400 ml) were harvested by centrifugation (1500 ***g***, 4°C, 5 min), and washed in 25 ml ice-cold lysis buffer (10 mM Tris-HCl, pH 7.5, 1 mM EDTA, 0.6 M sorbitol, 1 µg/ml pepstatin A, 0.1 mM phenylmethylsulfonyl fluoride, 1 mM dithiothreitol). After centrifugation, cells were resuspended in 4 ml of lysis buffer, and 2-ml aliquots were vortexed with glass beads (1.2 ***g***; 200 µm). The cell lysate was clarified by centrifugation (1000 ***g***, 10 min, 4°C), and plasma membrane-enriched membranes were subsequently

collected by centrifugation (9000 ***g***, 30 min, 4°C). Pellets were homogenized in 500 µl lysis buffer and centrifuged (1000 ***g***, 10 min, 4°C) before loading onto two-step sucrose gradients prepared in lysis buffer: 7.6 ml 43% w/w sucrose on top of 3.8 ml 53% w/w sucrose. After centrifugation (120,000 ***g***, 17 h, 4°C, rotor type Ti SW41), 1.2-ml fractions were collected from the top, diluted with 2 ml GTED20 and collected by centrifugation (100,000 ***g***, 1 h, 4°C) before resuspension in 40 µl SDS-loading buffer (0.3 M Tris-HCl pH 6.8, 37.5% v/v SDS 10%, 0.05 M DTT, 13% w/v sucrose, 25% w/v Bromophenol Blue, 0.01 M EDTA). Equal volumes per fraction (20 µl) were used for immunodetection.

Protein samples were loaded onto 8% acrylamide SDS-PAGE gels, transferred to nitrocellulose membranes, and immunodetected using antibodies targeting the yeast plasma membrane marker Pma1p (Monk et al., 1991), the Golgi marker Sed5p (Sapperstein, 1996), and the ER marker Dpm1p (Invitrogen, Carlsbad, CA, USA). A monoclonal mouse anti-RGSHis antibody (cat. no. 34650, Qiagen, Venlo, The Netherlands) was used to detect decahistidine-tagged proteins. GST was detected with a goat anti-GST antibody (cat. no. 27-4577-01, GE Healthcare, Brondby, Denmark). As secondary antibodies, a rabbit anti-mouse-IgG (Dako, Glostrup, DK), goat anti-rabbit-IgG (Dako, Glostrup, Denmark) and a polyclonal rabbit anti-goat-IgG (Sigma, St. Louis, MO, USA) conjugated to alkaline phosphatase were used. Commercially available antibodies were used at the recommended dilutions. All other antibodies were used at a 1:5000 dilution. Bands were visualized with the 5-bromo-4-chloro-3-indolyl phosphate/nitroblue tetrazolium (BCIP/NBT) color development substrate (Promega, Madison, WI, USA).

Drop test assays

For drop test assays, transformants were incubated in liquid SG medium for 4 h and then diluted with water to 0.1 and 0.01 OD_{600}/ml. Drops (5 µl) were spotted on plates and incubated at 30°C for 4 days. When indicated, papuamide A (Flintbox, LynseyHuxham; www.flintbox.com), was added to the medium at a final concentration of 0.75 µg/ml for the *quint* and *drs2Δdnf1,2,3Δ* mutants and 0.2 µg/ml for the triple *dnf1,2Δdrs2Δ* mutant. In tests using the quadruple *drs2Δdnf1,2,3Δ* mutant strain, selective SGF medium was used. Duramycin was used at a final concentration of 1.5 µM. All experiments were repeated independently at least three times.

NBD-lipid uptake assays

For NBD-lipid uptake experiments (Jensen et al., 2016a), yeast cells were grown in SD medium at 30°C and 110 rpm shaking for 18–24 h, and then transferred to 50 ml SG medium to an initial OD_{600}/ml of 0.009 for wild-type yeast or 0.03 for mutant strains. Cells were grown under the same conditions for another 16–17 h until early logarithmic phase (0.2-0.5 OD_{600}/ml). Cells were pelleted by centrifugation (700 ***g***, 10 min) and resuspended to 10 OD_{600}/ml in fresh SG medium and incubated for 5 min at 30°C before addition of 60 µM 1-palmitoyl-2-[NBD]-hexanoyl-*sn*-glycero-3-phosphocholine (NBD-PC), -phosphoethanolamine (NBD-PE), or -phosphoserine (NBD-PS) (Avanti Polar Lipids, Birmingham, AL, USA) from a 10 mM solution in DMSO. Cells were incubated at 30°C for 30 min with periodic mixing and subsequently washed twice in ice-cold SSA plus BSA medium (same as SG but without galactose and containing 2% w/v sorbitol, 20 mM NaN_3, and 3% w/v BSA) to extract NBD-lipids from the cell surface. Flow cytometry was performed on a Becton Dickinson FACS Calibur system (San Jose, CA, USA) equipped with an argon laser using Cell Quest software. Then, 1 µl of 1 mg/ml propidium iodide in water was added to 10^7 cells in 1 ml water just before analysis. A total of 20,000 cells were analyzed without gating during acquisition. Data were analyzed using FloJo software (Becton Dickinson, San Jose, CA, USA). A histogram of the red fluorescence (propidium iodide) was used to set the gate that excluded dead cells from the analysis. After scatter gating to exclude cells of abnormal morphology, the green fluorescence (NBD) of living cells was plotted on a histogram and the geometric mean fluorescence intensity of the population was calculated and normalized to an empty vector control. Experiments were repeated independently at least three times and the average normalized fluorescence intensity value for all experiments was calculated, together with the s.e.m.

Fluorescent protein visualization and image analysis

The protocol for SNAP labeling of yeast cells was adapted from Stagge et al. (2013). Cells were grown in 1 ml YPD medium at 30°C for 16–18 h with 150 rpm shaking to an OD_{600}/ml between 0.5 and 0.8, and harvested by centrifugation at 800 ***g*** for 2.5 min. After washing with deionized water, cells were resuspended in 100 µl SNAP-Cell Oregon Green solution (5 µM final concentration; New England Biolabs, Ipswich, MA, USA). The suspension was transferred to a 0.2 cm gap electroporation cuvette and cells were electroporated using an *E. coli* pulser ™ (Bio-Rad, Hercules, USA) with a pulse strength of 800 V. Immediately after electroporation, 400 µl YPD medium were added to the cells inside the cuvette. The suspension was transferred to a round-bottom culture vial and incubated at 30°C for 90 min under 150 rpm shaking. For identification of dead cells, Trypan Blue staining was carried out as previously described (Liesche et al., 2015). For imaging, cells were harvested, resuspended in 100 µl phosphate buffered saline (PBS; 137 mM NaCl, 2.7 mM KCl, 10 mM Na_2HPO_4, 1.8 mM KH_2PO_4, pH 7.4) and analyzed within 30 min. A Zeiss Elyra PS1 microscope (Zeiss, Jena, Germany) with a 100×/1.46 numerical aperture objective was used. Wide-field settings and detection with an Andor iXon 860 EMCCD camera (Andor Technology, Belfast, Ireland) provided the high sensitivity necessary to visualize the signal even in cells with very low intensity. Oregon Green was excited at 488 nm with 5 mW output laser power. The signal was detected through a 495–565 nm band pass emission filter. The exposure time was 300 ms and two times frame averaging was used to obtain images with sufficient signal-to-noise ratio.

All image processing and analysis was performed in ImageJ (National Institutes of Health, Bethesda, MD, USA). For determining the percentage of cells with Dnf3p-SNAP endomembrane signal versus those only showing plasma membrane signal, every cell on 10 images (5 to 20 cells per image) was visually analyzed and categorized into one of the four states shown in Fig. S1B. Dead cells, which constituted 20% of all cells, were identified by strong internal Trypan Blue signal and excluded from the analysis. The experiment was repeated three times with at least 50 cells being analyzed in each repetition. For the quantification of the Dnf3p–SNAP signal distribution, the signal background, which was the same on all images, was subtracted.

Cell morphology analysis, pseudohyphae formation and invasive growth

Wild-type and *Δdnf* yeast knockout cells were grown for 18–24 h in YPD at 30°C and 150 rpm shaking. Cultures were diluted in water to 0.1 OD_{600}/ml and drops (3 µl) were spotted onto agar plates lacking nitrogen or glucose. Colonies were imaged after incubation for 12 days at 30°C. A Leica MZ FLIII stereomicroscope (Leica microsystems, Wetzlar, Germany) with a transmitted light console base and 32× magnification was used. Petri plates were placed directly on the microscope stage. Imaging was done before and after washing under a stream of water. ImageJ was used for quantification of the outer ring size. For this, each image of a single pseudohyphal colony was divided into six equal quadrants starting on the vertical axis of the image. A measurement of the outer ring size was taken along each of the six quadrant-delimiting axes and the average of the six measurements was used as the final outer ring size for each colony.

To study cell elongation and pseudohyphal growth parameters, cells were incubated in YPD for 18–24 h and then transferred to medium without nitrogen (starting OD_{600}/ml 0.5) for another 18–24 h. Cultures were adjusted to 0.1 OD_{600}/ml with water before 100 µl culture was spread onto agar plates without nitrogen. Plates were incubated at 30°C for 12 h before imaging. Blocks of agar containing the spread cultures were lifted from the plate with a scalpel, transferred to a slide and cells were observed without a cover slip. For control experiments, yeast strains were grown in YPD for 18 h, washed in water and resuspended to 0.1 OD_{600}/ml in 2 ml complete SD medium. After 16 h, cells were mounted on microscopic slides for visualization. Light microscopy was performed with a Leica DMR HC microscope (Leica microsystems, Wetzlar, Germany) using a 100×/1.3 numerical aperture oil-immersion objective. Data were acquired for at least 900 cells per replicate for each yeast strain. Budding cells were treated as single cells. Any cell group containing three or more cells was considered a pseudohyphal colony.

Phylogenetic analysis

The collection of protein sequences for the phylogenetic analyses involved different steps. For the fungus-specific phylogenetic analysis, all P4 ATPases present in 37 fungal genomes, representing the major phylae of the fungal kingdom, were collected and curated as previously described (Palmgren et al., 2019). For the large analysis of eukaryotic P4 ATPases of various origins an extensive collection of P4 ATPases from the KEGG database was collected as previously described (Palmgren et al., 2019). To reduce the dataset, every sixth sequence in the collection was sampled and the rest discarded. As the KEGG database is biased towards dikaryote fungi (Ascomycota and Basidiomycota), the P4 ATPase sequences in the fungus-specific collection above (excluding those from dikaryote fungi) were added to the collection. Further sequences were collected from the NCBI database by two BLASTp searches performed with standard settings using the *S. cerevisiae* Dnf3p sequence (Uniprot Q12674) as a protein query. The first search was against the Non-Redundant Protein(NR) database excluding fungi, and the second against the fungi in the NR database excluding Ascomycota. Following both searches, the top 100 hits were collected and curated as described in Palmgren et al. (2019), and approved sequences were added to the sequence collection. The sequences in the final dataset were aligned using the MUSCLE algorithm (Edgar, 2004) in MEGA6 (Tamura et al., 2013) with standard settings except for a gap extension value of −5. The resulting alignment was analyzed using the GBLOCKS program, with a minimum of 376 positions for a conserved position, a minimum of 376 positions for a flank position, a maximum of 15 contiguous non-conserved positions, a minimum length of 2 for a block and gap positions allowed for half of the sequences. This resulted in an alignment of 600 positions in 55 blocks. The maximum likelihood analyses were performed employing RAxML 8.2.4 (Stamatakis, 2014) using the LG+G+I substitution model and involved 1000 rounds of bootstrapping. The analyses were run on the CIPRES Science Gateway (Miller et al., 2010) in the Extreme Science and Engineering Discovery Environment (XSEDE). Accession numbers for the proteins indicated in Fig. 8 are: *Arabidopsis thaliana*: ALA1, P98204; ALA2, P98205; ALA3, Q9XIE6; ALA4, Q9LNQ4; ALA5, Q9SGG3; ALA6, Q9SLK6; ALA7, Q9LVK9; ALA8, Q9LK90; ALA9, Q9SX33; ALA10, Q9LI83; ALA11, Q9SAF5; ALA12, P57792; *Saccharomyces cerevisiae*: Drs2p, P39524; Dnf1p, P32660; Dnf2p, Q12675; Dnf3p, Q12674; Neo1p, P40527; *Homo sapiens:* ATP8A1, Q9Y2Q0; ATP8A2, Q9NTI2; ATP8B1, O43520; ATP8B2, P98198; ATP8B3, O60423; AT8B4, Q8TF62; ATP9A, O75110; ATP9B, O43861; ATP10A, O60312; ATP10B, O94823; ATP10D, Q9P241; ATP11A, P98196; ATP11B, Q9Y2G3; ATP11C, Q8NB49.

Statistical analysis

All assays were performed in triplicates and data are presented as the mean± s.e.m., unless otherwise stated. For all assays except for the evaluation of the proportion of pseudohyphal colonies containing specific cell numbers, statistics were performed using a two-way ANOVA analysis with strains and biological replicates as the two variables followed by pairwise comparisons with Tukey adjusted *P*-values. $P<0.01$ was considered significant. For the distribution of pseudohyphal colony sizes within a population, pairwise comparisons were made with multinomial regression with strains and biological replicates as variables and *P*-values adjusted with Holm's method.

Acknowledgements

We gratefully acknowledge Stefan Jakobs (University Göttingen), Joost Holthius (University Osnabrüch), Kazuma Tanaka (Hokkaido University) and Anuj Kumar (University of Michigan) for generously providing plasmids and yeast strains. All bioimaging was carried out at the Center for Advanced Bioimaging Denmark (CAB).

Competing interests

The authors declare no competing or financial interests.

Author contributions

Conceptualization: M.M.F., S.R.C., T.G.P., R.L.L.-M.; Methodology: M.M.F., S.R.C., J.L., T.G.P., R.L.L.-M.; Software: S.N.; Formal analysis: M.M.F., S.R.C., J.L., J.T.O., S.H., S.N., H.S., M.P., T.G.P., R.L.L.-M.; Investigation: M.M.F., S.R.C., J.L., J.T.O., S.H., M.P., R.L.L.-M.; Resources: T.G.P., R.L.L.-M.; Data curation: J.T.O., S.H., M.P., R.L.L.-M.; Writing - original draft: M.M.F., S.R.C., J.L., J.T.O., M.P., T.G.P., R.L.L.-M.; Writing - review & editing: S.N., H.S., M.P., T.G.P., R.L.L.-M.; Visualization: J.L., R.L.L.-M.; Supervision: M.P., T.G.P., R.L.L.-M.; Project administration: T.G.P., R.L.L.-M.; Funding acquisition: M.P., T.G.P., R.L.L.-M.

Funding

This work was supported by the Danish Council for Independent Research, Natural Sciences (Det Frie Forskningsråd|Natur og Univers; FNU, grant number 1323-00297).

Data availability

All raw data from flow cytometry analysis, immunoblot scans and phenotypic characterization experiments can be found at Figshare.org under doi:10.6084/m9.figshare.8293730.v1

Supplementary information

Supplementary information available online at https://jcs.biologists.org/lookup/doi/10.1242/jcs.235994.supplemental

References

Alder-Baerens, N., Lisman, Q., Luong, L., Pomorski, T. and Holthuis, J. C. M. (2006). Loss of P4 ATPases Drs2p and Dnf3p disrupts aminophospholipid transport and asymmetry in yeast post-Golgi secretory vesicles. *Mol. Biol. Cell* **17**, 1632-1642. doi:10.1091/mbc.e05-10-0912

Andjelic, C. D., Planelles, V. and Barrows, L. R. (2008). Characterizing the anti-HIV activity of papuamide A. *Mar. Drugs* **6**, 528-549. doi:10.3390/md20080027

Anthonisen, A. N., Clausen, J. D. and Andersen, J. P. (2006). Mutational analysis of the conserved TGES loop of sarcoplasmic reticulum Ca^{2+}-ATPase. *J. Biol. Chem.* **281**, 31572-31582. doi:10.1074/jbc.M605194200

Atkins, B. D., Yoshida, S., Saito, K., Wu, C.-F., Lew, D. J. and Pellman, D. (2013). Inhibition of Cdc42 during mitotic exit is required for cytokinesis. *J. Cell Biol.* **202**, 231-240. doi:10.1083/jcb.201301090

Azouaoui, H., Montigny, C., Dieudonné, T., Champeil, P., Jacquot, A., Vázquez-Ibar, J. L., Le Maréchal, P., Ulstrup, J., Ash, M.-R., Lyons, J. A. et al. (2017). High phosphatidylinositol 4-phosphate (PI4P)-dependent ATPase activity for the Drs2p-Cdc50p flippase after removal of its N- and C-terminal extensions. *J. Biol. Chem.* **292**, 7954-7970. doi:10.1074/jbc.M116.751487

Baldridge, R. D., Xu, P. and Graham, T. R. (2013). Type IV P-type ATPases distinguish mono- versus di-acyl phosphatidylserine using a cytofacial exit gate in the membrane domain. *J. Biol. Chem.* **288**, 19516-19527. doi:10.1074/jbc.M113.476911

Balhadère, P. V. and Talbot, N. J. (2001). *PDE1* encodes a P-type ATPase involved in appressorium-mediated plant infection by the rice blast fungus *Magnaporthe grisea*. *Plant Cell* **13**, 1987-2004. doi:10.1105/tpc.13.9.1987

Brett, C. L., Kallay, L., Hua, Z., Green, R., Chyou, A., Zhang, Y., Graham, T. R., Donowitz, M. and Rao, R. (2011). Genome-wide analysis reveals the vacuolar pH-stat of Saccharomyces cerevisiae. *PLoS ONE* **6**, 1-9. doi:10.1371/journal.pone.0017619

Brown, M. W., Spiegel, F. W. and Silberman, J. D. (2009). Phylogeny of the "forgotten" cellular slime mold, *Fonticula alba*, reveals a key evolutionary branch within Opisthokonta. *Mol. Biol. Evol.* **26**, 2699-2709. doi:10.1093/molbev/msp185

Burgers, P. M. J. (1999). Overexpression of multisubunit replication factors in yeast. *Methods* **18**, 349-355. doi:10.1006/meth.1999.0796

Ceccato-antonini, S. R. and Sudbery, P. E. (2004). Filamentous growth in *Saccharomyces cerevisiae*. *Brazilian J. Microbiol.* **35**, 173-181. doi:10.1590/S1517-83822004000200001

Chantalat, S., Park, S.-K., Hua, Z. L., Liu, K., Gobin, R., Peyroche, A., Rambourg, A., Graham, T. R. and Jackson, C. L. (2004). The Arf activator Gea2p and the P-type ATPase Drs2p interact at the golgi in *Saccharomyces cerevisiae*. *J. Cell Sci.* **117**, 711-722. doi:10.1242/jcs.00896

Chen, C.-Y., Ingram, M. F., Rosal, P. H. and Graham, T. R. (1999). Role for Drs2p, a P-type ATPase and potential aminophospholipid translocase, in yeast late Golgi function. *J. Cell Biol.* **147**, 1223-1236. doi:10.1083/jcb.147.6.1223

Edgar, R. C. (2004). MUSCLE: multiple sequence alignment with high accuracy and high throughput. *Nucleic Acid Res.* **32**, 1792-1797. doi:10.1093/nar/gkh340

Fairn, G. D., Hermansson, M., Somerharju, P. and Grinstein, S. (2011). Phosphatidylserine is polarized and required for proper Cdc42 localization and for development of cell polarity. *Nat. Cell Biol.* **13**, 1424-1430. doi:10.1038/ncb2351

Furuta, N., Fujimura-Kamada, K., Saito, K., Yamamoto, T. and Tanaka, K. (2007). Endocytic recycling in yeast is regulated by putative phospholipid translocases and the Ypt31p/32p-Rcy1p pathway. *Mol. Biol. Cell* **18**, 295-312. doi:10.1091/mbc.e06-05-0461

Gietz, R. D. and Woods, R. A. (2002). Transformation of yeast by lithium acetate/single-stranded carrier DNA/polyethylene glycol method. *Methods Enzymol.* **350**, 87-96. doi:10.1016/S0076-6879(02)50957-5

Gilbert, M. J., Thornton, C. R., Wakley, G. E. and Talbot, N. J. (2006). A P-type ATPase required for rice blast disease and induction of host resistance. *Nature* **440**, 535-539. doi:10.1038/nature04567

Hachiro, T., Yamamoto, T., Nakano, K. and Tanaka, K. (2013). Phospholipid flippases Lem3p-Dnf1p and Lem3p-Dnf2p are involved in the sorting of the tryptophan permease Tat2p in yeast. *J. Biol. Chem.* **288**, 3594-3608. doi:10.1074/jbc.M112.416263

Hanks, S. K., Quinn, A. M. and Hunter, T. (1988). The protein kinase family: conserved features and deduced phylogeny of the catalytic domains. *Science* **241**, 42-52. doi:10.1126/science.3291115

Hua, Z. L. and Graham, T. R. (2003). Requirement for Neo1p in retrograde transport from the Golgi complex to the endoplasmic reticulum. *Mol. Biol. Cell* **14**, 4971-4983. doi:10.1091/mbc.e03-07-0463

Hua, Z., Fatheddin, P. and Graham, T. R. (2002). An essential subfamily of Drs2p-related P-Type ATPases is required for protein trafficking between Golgi complex and endosomal/vacuolar system. *Mol. Biol. Cell* **13**, 3162-3177. doi:10.1091/mbc.e02-03-0172

Jensen, M. S., Costa, S., Günther-Pomorski, T. and López-Marqués, R. L. (2016a). Cell-based lipid flippase assay employing fluorescent lipid derivatives. *Methods Mol. Biol.* **1377**, 371-382. doi:10.1007/978-1-4939-3179-8_33

Jensen, M. S., Costa, S. R., Theorin, L., Christensen, J. P., Pomorski, T. G. and López-Marqués, R. L. (2016b). Application of image cytometry to characterize heterologous lipid flippases in yeast. *Cytom. Part A* **89**, 673-680. doi:10.1002/cyto.a.22886

Johnson, C., Kweon, H. K., Sheidy, D., Shively, C. A., Mellacheruvu, D., Nesvizhskii, A. I., Andrews, P. C. and Kumar, A. (2014). The yeast Sks1p kinase signaling network regulates pseudohyphal growth and glucose response. *PLoS Genet.* **10**, e1004183. doi:10.1371/journal.pgen.1004183

Karunanithi, S. and Cullen, P. J. (2012). The filamentous growth MAPK pathway responds to glucose starvation through the Mig1/2 transcriptional repressors in *Saccharomyces cerevisiae*. *Genetics* **192**, 869-887. doi:10.1534/genetics.112.142661

Kato, U., Emoto, K., Fredriksson, C., Nakamura, H., Ohta, A., Kobayashi, T., Murakami-Murofushi, K., Kobayashi, T. and Umeda, M. (2002). A novel membrane protein, Ros3p, is required for phospholipid translocation across the plasma membrane in *Saccharomyces cerevisiae*. *J. Biol. Chem.* **277**, 37855-37862. doi:10.1074/jbc.M205564200

Kiss, E., Hegedüs, B., Virágh, M., Varga, T., Merényi, Z., Kószó, T., Bálint, B., Prasanna, A. N., Krizsán, K., Kocsubé, S. et al. (2019). Comparative genomics reveals the origin of fungal hyphae and multicellularity. *Nat. Commun.* **10**, 4080. doi:10.1038/s41467-019-12085-w

Lamping, E., Tanabe, K., Niimi, M., Uehara, Y., Monk, B. C. and Cannon, R. D. (2005). Characterization of the *Saccharomyces cerevisiae sec6-4*^{1} mutation and tools to create *S. cerevisiae* strains containing the *sec6*-4 allele. *Gene* **361**, 57-66. doi:10.1016/j.gene.2005.07.014

Lenoir, G., Williamson, P., Puts, C. F. and Holthuis, J. C. M. (2009). Cdc50p plays a vital role in the ATPase reaction cycle of the putative aminophospholipid transporter Drs2p. *J. Biol. Chem.* **284**, 17956-17967. doi:10.1074/jbc.M109.013722

Liesche, J., Marek, M. and Günther-Pomorski, T. (2015). Cell wall staining with Trypan blue enables quantitative analysis of morphological changes in yeast cells. *Front. Microbiol.* **6**, 107. doi:10.3389/fmicb.2015.00107

Lo, W.-C., Lee, M. E., Narayan, M., Chou, C.-S. and Park, H.-O. (2013). Polarization of diploid daughter cells directed by spatial cues and GTP hydrolysis of Cdc42 budding yeast. *PLoS ONE* **8**, e56665. doi:10.1371/journal.pone.0056665

López-Marqués, R. L., Poulsen, L. R., Hanisch, S., Meffert, K., Buch-Pedersen, M. J., Jakobsen, M. K., Pomorski, T. G. and Palmgren, M. G. (2010). Intracellular targeting signals and lipid specificity determinants of the ALA/ALIS P4-ATPase complex reside in the catalytic ALA alpha-subunit. *Mol. Biol. Cell* **21**, 791-801. doi:10.1091/mbc.e09-08-0656

López-Marqués, R. L., Holthuis, J. C. M. and Pomorski, T. G. (2011). Pumping lipids with P4-ATPases. *Biol. Chem.* **392**, 67-76. doi:10.1515/bc.2011.015

López-Marqués, R. L., Poulsen, L. R. and Palmgren, M. G. (2012). A putative plant aminophospholipid flippase, the arabidopsis P4 ATPase ALA1, localizes to the plasma membrane following association with a β-subunit. *PLoS ONE* **7**, e33042. doi:10.1371/journal.pone.0033042

López-Marqués, R. L., Theorin, L., Palmgren, M. G. and Pomorski, T. G. (2014). P4-ATPases: lipid flippases in cell membranes. *Pflügers Arch. Eur. J. Physiol.* **466**, 1227-1240. doi:10.1007/s00424-013-1363-4

Miller, M. A., Pfeiffer, W. and Schwartz, T. (2010). Creating the CIPRES Science Gateway for inference of large phylogenetic trees. In *Gateway Computing Environments Workshop (GCE)*, pp. 1-8. New Orleans, LA.

Monk, B. C., Montesinos, C., Ferguson, C., Leonard, K. and Serrano, R. (1991). Immunological approaches to the transmembrane topology and conformational changes of the carboxyl-terminal regulatory domain of yeast plasma membrane H(+)-ATPase. *J. Biol. Chem.* **266**, 18097-18103.

Nakano, K., Yamamoto, T., Kishimoto, T., Noji, T. and Tanaka, K. (2008). Protein kinases Fpk1p and Fpk2p are novel regulators of phospholipid asymmetry. *Mol. Biol. Cell* **19**, 1783-1797. doi:10.1091/mbc.e07-07-0646

Natarajan, P., Liu, K., Patil, D. V., Sciorra, V. A., Jackson, C. L. and Graham, T. R. (2009). Regulation of a Golgi flippase by phosphoinositides and an ArfGEF. *Nat. Cell Biol.* **11**, 1421-1426. doi:10.1038/ncb1989

Orlando, K., Zhang, J., Zhang, X., Yue, P., Chiang, T., Bi, E. and Guo, W. (2008). Regulation of Gic2 localization and function by phosphatidylinositol 4,5-bisphosphate during the establishment of cell polarity in budding yeast. *J. Biol. Chem.* **283**, 14205-14212. doi:10.1074/jbc.M708178200

Palmgren, M., Østerberg, J. T., Nintemann, S. J., Poulsen, L. R. and López-Marqués, R. L. (2019). Evolution and a revised nomenclature of P4 ATPases, a eukaryotic family of lipid flippases. *Biochim. Biophys. Acta Biomembr.* **1861**, 1135-1151. doi:10.1016/j.bbamem.2019.02.006

Parsons, A. B., Lopez, A., Givoni, I. E., Williams, D. E., Gray, C. A., Porter, J., Chua, G., Sopko, R., Brost, R. L., Ho, C.-H. et al. (2006). Exploring the mode-of-action of bioactive compounds by chemical-genetic profiling in yeast. *Cell* **126**, 611-625. doi:10.1016/j.cell.2006.06.040

Pomorski, T., Lombardi, R., Riezman, H., Devaux, P. F., van Meer, G. and Holthuis, J. C. M. (2003). Drs2p-related P-type ATPases Dnf1p and Dnf2p are required for phospholipid translocation across the yeast plasma membrane and serve a role in endocytosis. *Mol. Biol. Cell* **14**, 1240-1254. doi:10.1091/mbc.e02-08-0501

Poulsen, L. R., López-Marqués, R. L., McDowell, S. C., Okkeri, J., Licht, D., Schulz, A., Pomorski, T., Harper, J. F. and Palmgren, M. G. (2008). The Arabidopsis P4-ATPase ALA3 localizes to the Golgi and requires a β-Subunit to function in lipid translocation and secretory vesicle formation. *Plant Cell* **20**, 658-676. doi:10.1105/tpc.107.054767

Poulsen, L. R., López-Marqués, R. L., Pedas, P. R., McDowell, S. C., Brown, E., Kunze, R., Harper, J. F., Pomorski, T. G. and Palmgren, M. (2015). A phospholipid uptake system in the model plant *Arabidopsis thaliana*. *Nat. Commun.* **6**, 7649. doi:10.1038/ncomms8649

Pryciak, P. M. and Huntress, F. A. (1998). Membrane recruitment of the kinase cascade scaffold protein Ste5 by the GBy complex underlies activation of the yeast pheromone response pathway. *Genes Dev.* **12**, 2684-2697. doi:10.1101/gad.12.17.2684

Riekhof, W. R. and Voelker, D. R. (2006). Uptake and utilization of lyso-phosphatidylethanolamine by Saccharomyces cerevisiae. *J. Biol. Chem.* **281**, 36588-36596. doi:10.1074/jbc.M608851200

Riekhof, W. R. and Voelker, D. R. (2009). The yeast plasma membrane P4-ATPases are major transporters for lysophospholipids. *Biochim. Biophys. Acta Mol. Cell Biol. Lipids* **1791**, 620-627. doi:10.1016/j.bbalip.2009.02.013

Roelants, F. M., Torrance, P. D., Bezman, N. and Thorner, J. (2002). Pkh1 and Pkh2 differentially phosphorylate and activate Ypk1 and Ykr2 and define protein kinase modules required for maintenance of cell wall integrity. *Mol. Biol. Cell* **13**, 3005-3028. doi:10.1091/mbc.e02-04-0201

Roelants, F. M., Baltz, A. G., Trott, A. E., Fereres, S. and Thorner, J. (2010). A protein kinase network regulates the function of aminophospholipid flippases. *Proc. Natl. Acad. Sci. USA* **107**, 34-39. doi:10.1073/pnas.0912497106

Roelants, F. M., Su, B. M., von Wulffen, J., Ramachandran, S., Sartorel, E., Trott, A. E. and Thorner, J. (2015). Protein kinase Gin4 negatively regulates flippase function and controls plasma membrane asymmetry. *J. Cell Biol.* **208**, 299-311. doi:10.1083/jcb.201410076

Roland, B. P., Naito, T., Best, J. T., Arnaiz-Yépez, C., Takatsu, H., Yu, R. J., Shin, H. W., and Graham, T. R. (2019). Yeast and human P4-ATPases transport glycosphingolipids using conserved structural motifs. *J. Biol. Chem.* **294**, 1794-1806. doi:10.1074/jbc.RA118.005876

Saito, K., Fujimura-Kamada, K., Furuta, N., Kato, U., Umeda, M. and Tanaka, K. (2004). Cdc50p, a protein required for polarized growth, associates with the Drs2p P-Type ATPase implicated in phospholipid translocation in *Saccharomyces cerevisiae*. *Mol. Biol. Cell* **15**, 3418-3432. doi:10.1091/mbc.e03-11-0829

Saito, K., Fujimura-Kamada, K., Hanamatsu, H., Kato, U., Umeda, M., Kozminski, K. G. and Tanaka, K. (2007). Transbilayer phospholipid flipping regulates Cdc42p signaling during polarized cell growth via Rga GTPase-activating proteins. *Dev. Cell* **13**, 743-751. doi:10.1016/j.devcel.2007.09.014

Sapperstein, S. K. (1996). Assembly of the ER to Golgi SNARE complex requires Uso1p. *J. Cell Biol.* **132**, 755-767. doi:10.1083/jcb.132.5.755

Sartorel, E., Barrey, E., Lau, R. K. and Thorner, J. (2015). Plasma membrane aminoglycerolipid flippase function is required for signaling competence in the yeast mating pheromone response pathway. *Mol. Biol. Cell* **26**, 134-150. doi:10.1091/mbc.e14-07-1193

Sauer, B. (1987). Functional Expression of the cre-lox site-specific recombination system in the yeast *Saccharomyces cerevisiae*. *Mol. Cell. Biol.* **7**, 2087-2096. doi:10.1128/MCB.7.6.2087

Schultzhaus, Z., Yan, H. and Shaw, B. D. (2015). *Aspergillus nidulans* flippase DnfA is cargo of the endocytic collar and plays complementary roles in growth and phosphatidylserine asymmetry with another flippase, DnfB. *Mol. Microbiol.* **97**, 18-32. doi:10.1111/mmi.13019

Schultzhaus, Z., Cunningham, G. A., Mouriño-Pérez, R. R. and Shaw, B. D. (2019). The phospholipid flippase DnfD localizes to late Golgi and is involved in asexual differentiation in *Aspergillus nidulans*. *Mycologia* **00**, 1-13. doi:10.1080/00275514.2018.1543927

Sebastian, T. T., Baldridge, R. D., Xu, P. and Graham, T. R. (2012). Phospholipid flippases: Building asymmetric membranes and transport vesicles. *Biochim. Biophys. Acta* **1821**, 1068-1077. doi:10.1016/j.bbalip.2011.12.007

Song, Q. and Kumar, A. (2012). An overview of autophagy and yeast pseudohyphal growth: Integration of signaling pathways during nitrogen stress. *Cells* **1**, 263-283. doi:10.3390/cells1030263

Stagge, F., Mitronova, G. Y., Belov, V. N., Wurm, C. A. and Jakobs, S. (2013). Snap-, CLIP- and Halo-tag labelling of budding yeast cells. *PLoS ONE* **8**, e78745. doi:10.1371/journal.pone.0078745

Stamatakis, A. (2014). RAxML version 8: a tool for phylogenetic analysis and post-analysis of large phylogenies. *Bioinformatics* **30**, 1312-1313. doi:10.1093/bioinformatics/btu033

Stevens, H. C., Malone, L. and Nichols, J. W. (2008). The putative aminophospholipid translocases, *DNF1* and *DNF2*, are not required for 7-Nitrobenz-2-oxa-1,3-diazol-4-yl-phosphatidylserine flip across the plasma membrane of Saccharomyces cerevisiae. *J. Biol. Chem.* **283**, 35060-35069. doi:10.1074/jbc.M802379200

Takar, M., Wu, Y. and Graham, T. R. (2016). The essential Neo1 protein from budding yeast plays a role in establishing aminophospholipid asymmetry of the plasma membrane. *J. Biol. Chem.* **291**, 15727-15739. doi:10.1074/jbc.M115.686253

Tamura, K., Stecher, G., Peterson, D., Filipski, A. and Kumar, S. (2013). MEGA6: Molecular Evolutionary Genetics Analysis version 6.0. *Mol. Biol. Evol.* **30**, 2725-2729. doi:10.1093/molbev/mst197

Tong, Z., Gao, X.-D., Howell, A. S., Bose, I., Lew, D. J. and Bi, E. (2007). Adjacent positioning of cellular structures enabled by a Cdc42 GTPase-activating protein-mediated zone of inhibition. *J. Cell Biol.* **179**, 1375-1384. doi:10.1083/jcb.200705160

Tsai, P.-C., Hsu, J.-W., Liu, Y.-W., Chen, K.-Y. and Lee, F.-J. S. (2013). Arl1p regulates spatial membrane organization at the trans-Golgi network through interaction with Arf-GEF Gea2p and flippase Drs2p. *Proc. Natl. Acad. Sci. USA* **110**, E668-E677. doi:10.1073/pnas.1221484110

van Meer, G. (2011). Dynamic transbilayer lipid asymmetry. *Cold Spring Harb. Perspect. Biol.* **3**, a004671-a004671. doi:10.1101/cshperspect.a004671

Villalba, J. M., Palmgren, M. G., Berberian, G. E., Ferguson, C. and Serrano, R. (1992). Functional expression of plant plasma membrane H^+-ATPase in yeast endoplasmic reticulum. *J. Biol. Chem.* **267**, 12341-12349.

Wicky, S., Schwarz, H. and Singer-Krüger, B. (2004). Molecular interactions of yeast Neo1p, an essential member of the Drs2 family of aminophospholipid translocases, and its role in membrane trafficking within the endomembrane system. *Mol. Cell. Biol.* **24**, 7402-7418. doi:10.1128/MCB.24.17.7402-7418.2004

Wu, Y., Takar, M., Cuentas-Condori, A. A. and Graham, T. R. (2016). Neo1 and phosphatidylethanolamine contribute to vacuole membrane fusion in *Saccharomyces cerevisiae*. *Cell. Logist.* **6**, e1228791. doi:10.1080/21592799.2016.1228791

Xu, P., Baldridge, R. D., Chi, R. J., Burd, C. G. and Graham, T. R. (2013). Phosphatidylserine flipping enhances membrane curvature and negative charge required for vesicular transport. *J. Cell Biol.* **202**, 875-886. doi:10.1083/jcb.201305094

Yakir-Tamang, L. and Gerst, J. E. (2009). A phosphatidylinositol-transfer protein and phosphatidylinositol-4-phosphate 5-kinase control Cdc42 to regulate the actin cytoskeleton and secretory pathway in yeast. *Mol. Biol. Cell* **20**, 3583-3597. doi:10.1091/mbc.e08-10-1073

Zachowski, A. (2012). New insights in membrane lipid asymmetry in animal and plant cells. In *Transmembrane Dynamics of Lipids* (ed. P. F. Devaux and A. Herrmann), pp. 45-64. Hoboken, NJ, USA: John Wiley & Sons, Inc.

Zhou, X., Sebastian, T.T. and Graham, T.R. (2013). Auto-inhibition of Drs2p, a yeast phospholipid flippase, by its carboxyl-terminal tail. *J. Biol. Chem.* **288**, 31807-31815. doi:10.1074/jbc.M113.481986

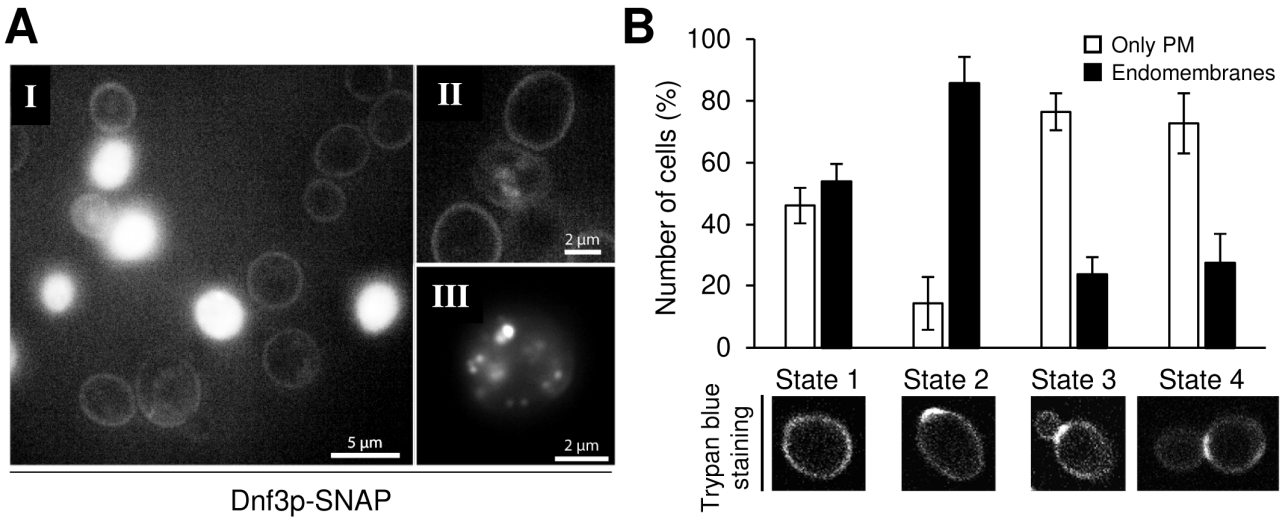

Figure S1. Dnf3p reaches the plasma membrane in a cell-cycle-dependent manner. (A) Wild-type yeast (BY4741) cells carrying a genomic SNAP-tagged version of Dnf3p (I, II) or Abp1p (III) were labeled by electroporation with the SNAP-substrate Oregon Green before imaging by confocal microscopy. **B**) After Dnf3p-SNAP labeling with Oregon green, cells were stained with trypan blue to visualize the cell wall and divided into four budding-related states. *Upper panel,* Relative number of cells showing Dnf3p-SNAP signal at the plasma membrane versus internal membranes. Results are given as mean ± SD for at least 50 cells. Statistical analysis was done using Student's *t*-test. A value $p < 0.05$ was considered statistically significant. *Lower panel,* Examples of trypan Blue-stained cells in different states of growth. State 1 includes non-budding cells with uniform cell wall staining; State 2 comprises cells that show a localized thickening of the cell wall at the site of future bud emergence; State 3 cells are characterized by the presence of a clearly growing bud and a thickening of the cell wall around the bud neck; State 4 defines all cells assumed to be approaching cytokinesis in which mother and daughter cells are close in size but remain attached by a bud neck with a thickened cell wall.

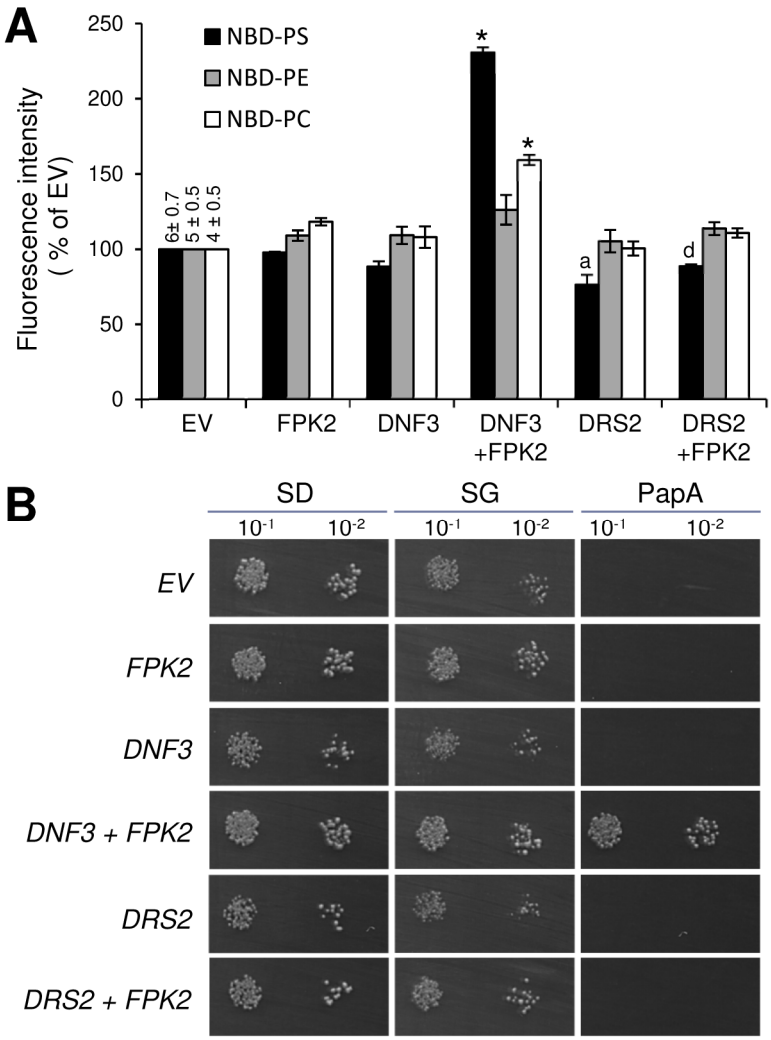

Figure S2. Overexpression of *DNF3* and *FPK2*, but not *DRS2* and *FPK2*, results in PS transport at the plasma membrane. *fpk1,2Δdnf1,2,3Δ* cells transformed with either empty vectors (EV) or expression plasmids carrying *DNF3* or *DRS2* alone or in combination with *FPK2* were analysed for (**A**) NBD-lipid uptake, (**B**) functional complementation of the papuamide A-sensitive growth defect. Results in panel A represent the means ± SEM from at least three independent experiments. Numbers above the bars represent mean fluorescence values (± SEM) in arbitrary units. Statistical significance according to an ANOVA test ($p<0.01$) is given in small letters for all strains except the empty vector control: a, statistically significant with respect to the empty vector; b, statistically significant with respect to *FPK2*; c, statistically significant with respect to DNF3; d, statistically significant with respect to *DRS2*. In panel B, two serial cell dilutions were spotted onto glucose- (SD) or galactose containing (SG, Induced expression) plates, supplemented with 0.75 µg/mL papuamide A (PapA) as indicated. Numbers indicate cell dilution.

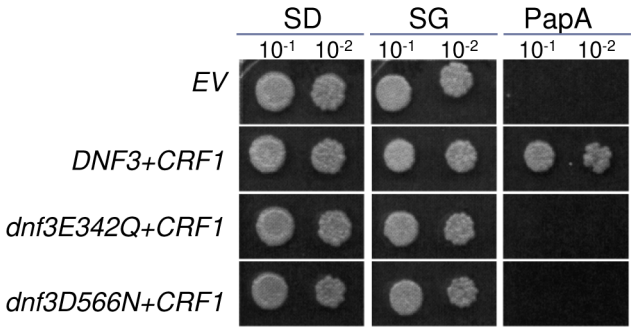

Figure S3. Fpk1p acts upstream of Dnf3p. *fpk1,2Δdnf1,2,3Δ (quint)* cells transformed with either empty vectors (EV) or expression plasmids carrying *DNF3* or catalytically inactive *dnf3* mutants alone or in combination with *CRF1* were spotted in two serial dilutions onto glucose- (SD) or galactose containing (SG) plates, supplemented with 0.75 µg/mL papuamide A (PapA) as indicated. Numbers indicate cell dilution.

Journal of Cell Science • Supplementary information

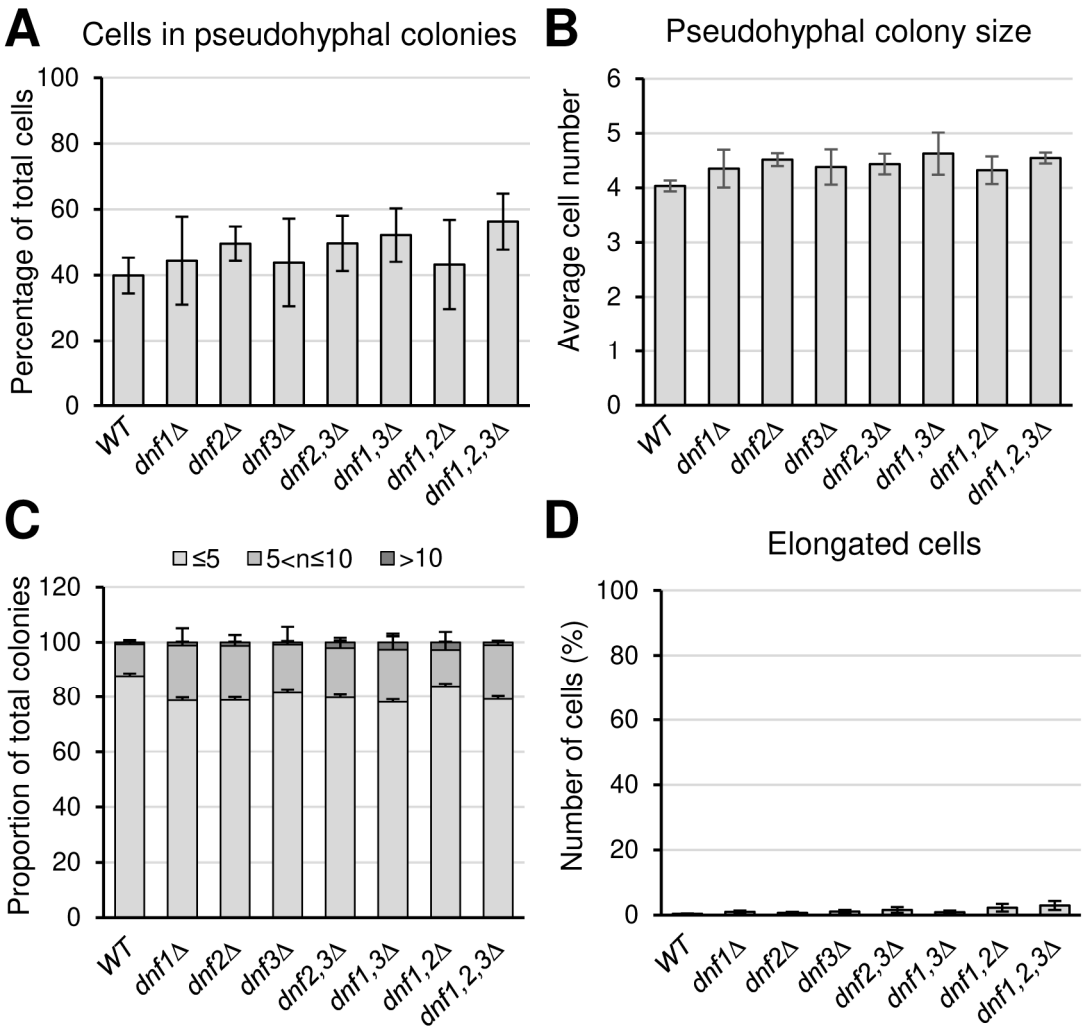

Figure S4. Deletion of *DNF* genes in diploid yeast cells does not result in significant phenotypes under standard growth conditions. Yeast wild-type and *DNF* knockout diploid cells were grown in liquid SD media containing all auxotrophic nutrients for 15 hours before microscopic visualization. The number of abnormally elongated cells (A) and the number of cells forming pseudohyphal colonies (B) were counted. Pseudohyphal colony growth was characterized by the average number of cells forming the colony (C) and the proportion of colonies with a specific number (n) of cells (D). Results are averages ± SEM from at least three independent experiments. At least 900 single cells (including budding cells) and pseudohyphal colonies with 3 or more cells were counted. No significant differences were identified according to the statistical analyses described in materials and methods.

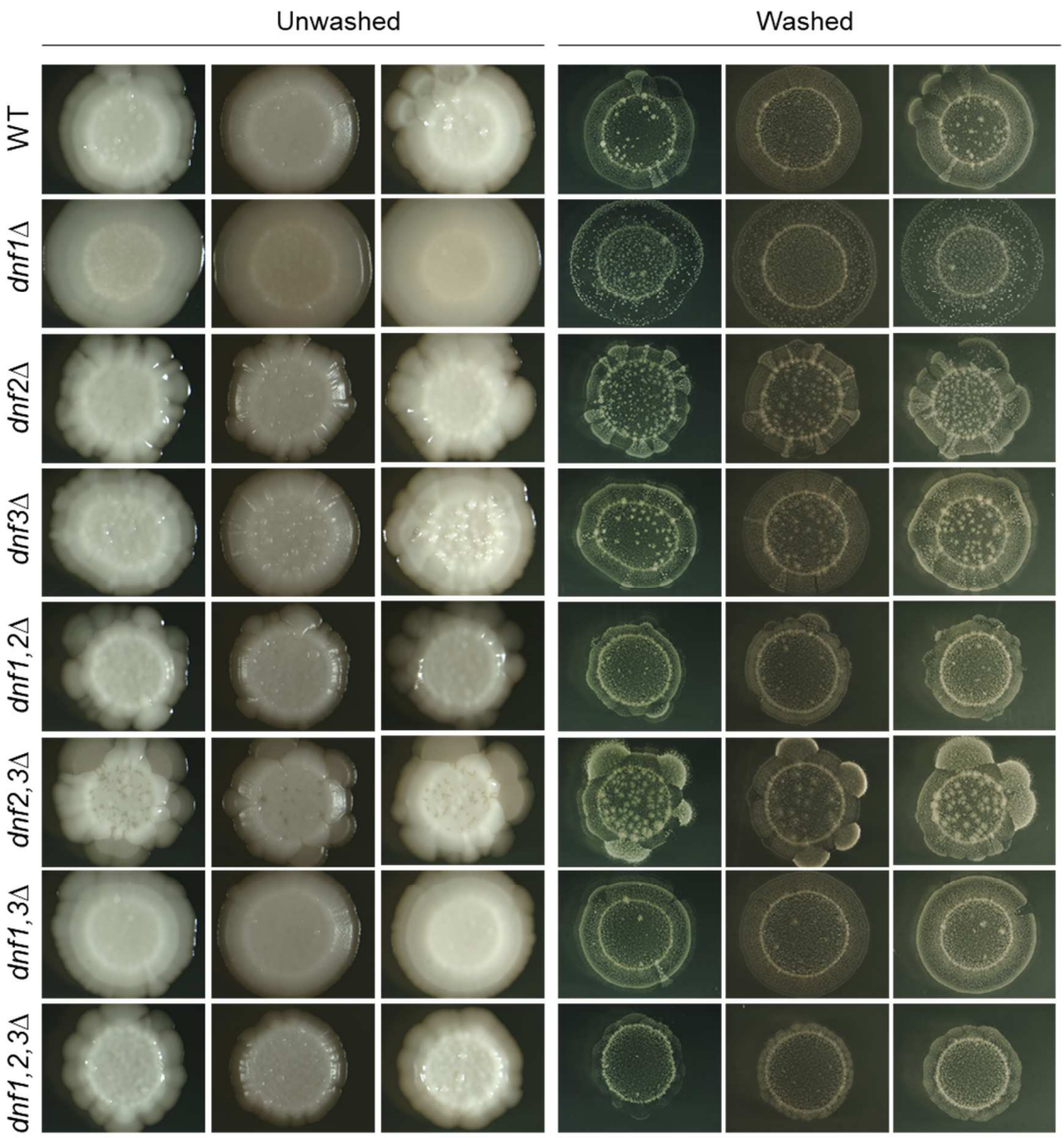

Figure S5. Morphological and penetration defects of pseudohyphal colonies in *dfnΔ* mutant strains. Yeast wild-type and *DNF* knockout cells were spotted onto plates without glucose. Plates were observed at the microscope after 12 d incubation and images were taken before and after wash with water to study pseudohyphal colony morphology and pseudophyphae invasiveness, respectively. Colonies from three independent biological replicates are shown for comparison.

Journal of Cell Science • Supplementary information

Table S1. Yeast strains used in this study.

Strain	Genotype	Source
KKT61	*MATa LYS2 ura3Δ0 his3Δ1 leu2Δ0 MET15*	(Nakano et al., 2008)
KKT268	*MATa LYS2 ura3Δ0 his3Δ1 leu2Δ0 MET15 fpk1::HphMX4 fpk2::KanMX6*	(Nakano et al., 2008)
MP3677	*MATa LYS2 ura3Δ0 his3Δ1 leu2Δ0 MET15 fpk1Δ::HphMX4 fpk2Δ::KanMX6 Δdnf1::LoxP Δdnf2::LoxP*	This study
MP3678	*MATa LYS2 ura3Δ0 his3Δ1 leu2Δ0 MET15 fpk1Δ::HphMX4 fpk2Δ::KanMX6 Δdnf1::LoxP Δdnf2::LoxP Δdnf3::LoxP*	This study
TPY127	*MATα sec6-4, TPI1::SUC2::TRP1, ura-52 his3-Δ200 leu2-3, -112, trp1-1, drs2::LoxP dnf1::LoxP dnf2::LoxP dnf3::LoxP*	(Alder-Baerens et al., 2006)
ZHY709	*MATa his3 leu2 ura3 met15 dnf1Δ dnf2Δ drs2::LEU2*	(Hua et al., 2002)
BY4741	*MATa his3Δ1 leu2Δ0 met15Δ0 ura3Δ0*	EUROSCARF
BY4741 Abp1-SNAP	*MATa his3Δ1 leu2Δ0 met15Δ0 ura3Δ0 ABP1-SNAP::KanMX*	(Stagge et al., 2013)
BY4741 Dnf3-SNAP	*MATa his3Δ1 leu2Δ0 met15Δ0 ura3Δ0 DNF3-SNAP::HIS3*	This study
TPY52	*MAT*a *ura3-52 his3-Δ200 leu2-3,112 trp1-Δ901 ade2-101 suc2-Δ9 Δbar1::URA3*	This study
TPY60	*MAT*a *ura3-52 his3-Δ200 leu2-3,112 trp1-Δ901 ade2-101 suc2-Δ9 Δbar1::URA3 Δdnf1::loxP Δdnf2::loxP*	This study
TPY134	*MAT*a *ura3-52 his3-Δ200 leu2-3,112 trp1-Δ901 ade2-101 suc2-Δ9 Δbar1::URA3 Δdnf1::loxP Δdnf2::loxP Δdnf3::loxP HIS3-loxP*	This study
TPY116	*MAT*a *ura3-52 his3-Δ200 leu2-3,112 trp1-Δ901 ade2-101 suc2-Δ9 Δbar1::URA3 Δdnf1::loxP Δdnf2::loxP Δdrs2::loxP*	This study
For cell elongation, hyphae formation and invasive growth studies		
Y825	*MAT**a** ura3-52 leu2_0*	(Johnson et al., 2014)
HLY337	*MAT**α** ura3-52 trp1-1*	(Johnson et al., 2014)
MP5053	*MAT**a** ura3-52 leu2_0 Δdnf*1::loxP	This study
MP5054	*MAT**α** ura3-52 trp1-1 Δdnf*1::loxP	This study
MP5055	*MAT**a** ura3-52 leu2_0 Δdnf*2::loxP	This study
MP5056	*MAT**α** ura3-52 trp1-1 Δdnf*2::loxP	This study
MP5057	*MAT**a** ura3-52 leu2_0 Δdnf*3::loxP	This study
MP5058	*MAT**α** ura3-52 trp1-1 Δdnf*3::loxP	This study
MP5069	*MAT**a** ura3-52 leu2_0 Δdnf*2::loxP *Δdnf*3::loxP	This study
MP5070	*MAT**α** ura3-52 trp1-1 Δdnf*2::loxP *Δdnf*3::loxP	This study
MP5071	*MAT**a** ura3-52 leu2_0 Δdnf*3::loxP *Δdnf1*::loxP	This study
MP5072	*MAT**α** ura3-52 trp1-1 Δdnf*3::loxP *Δdnf1*::loxP	This study
MP5073	*MAT**a** ura3-52 leu2_0 Δdnf*2::loxP *Δdnf1*::loxP	This study

Journal of Cell Science • Supplementary information

MP5074	*MATα ura3-52 trp1-1 Δdnf2*::loxP *Δdnf1*::loxP	This study
MP5080	*MATα ura3-52 leu2_0 Δdnf2*::loxP *Δdnf3*::loxP *Δdnf1*::loxP	This study
MP5081	*MATα ura3-52 trp1-1 Δdnf2*::loxP *Δdnf3*::loxP *Δdnf1*::loxP	This study
MP5065	*MATa /MATα ura3-52/ura3-52 leu2_0/LEU2 TRP1/ trp1-1*	This study
MP5066	*MATa /MATα ura3-52/ura3-52 leu2_0/LEU2 TRP1/ trp1-1 Δdnf1*::loxP/ *Δdnf1*::loxP	This study
MP5067	*MATa /MATα ura3-52/ura3-52 leu2_0/LEU2 TRP1/ trp1-1 Δdnf2*::loxP/ *Δdnf2*::loxP	This study
MP5068	*MATa /MATα ura3-5/ura3-522 leu2_0/LEU2 TRP1/ trp1-1 Δdnf3*::loxP/ *Δdnf3*::loxP	This study
MP5075	*MATa /MATα ura3-52/ura3-52 leu2_0/LEU2 TRP1/ trp1-1 Δdnf2*::loxP/ *Δdnf2*::loxP *Δdnf3*::loxP/*Δdnf3*::loxP	This study
MP5076	*MATa /MATα ura3-52/ura3-52 leu2_0/LEU2 TRP1/ trp1-1 Δdnf1*::loxP/ *Δdnf1*::loxP *Δdnf3*::loxP/*Δdnf3*::loxP	This study
MP5077	*MATa /MATα ura3-52/ura3-52 leu2_0/LEU2 TRP1/ trp1-1 Δdnf1*::loxP/ *Δdnf1*::loxP *Δdnf2*::loxP/*Δdnf2*::loxP	This study
MP5082	*MATa /MATα ura3-52/ura3-52 leu2_0/LEU2 TRP1/ trp1-1 Δdnf1*::loxP/ *Δdnf1*::loxP *Δdnf2*::loxP/*Δdnf2*::loxP *Δdnf3*::loxP/*Δdnf3*::loxP	This study

Journal of Cell Science • Supplementary information

Table S2. Plasmids used in this study.

Name	Backbone	Insert[1]	Selection	Promoter	Reference
pMP1965	pRS423-GAL	Gateway® Reading Frame Cassette A	*HIS3*	GAL1-10	(Poulsen et al., 2008)
pRS425-GAL		None	*LEU2*	GAL1-10	(Burgers, 1999)
pRS423-GAL		None	*HIS3*	GAL1-10	(Burgers, 1999)
pMP2340	pRS423-GAL	*DRS2*	*HIS3*	GAL1-10	(Poulsen et al., 2008)
pMP2355	pRS425-GAL	Gateway® Reading Frame Cassette C	*LEU2*	GAL1-10	This study
pMP3129	pMP423-GAL	*yeGFP*	*HIS3*	GAL1-10	This study
pMP3164	pMP3129	*yeGFP-DRS2*	*HIS3*	GAL1-10	This study
pMP3714	pRS425-GAL	*FPK2*	*LEU2*	GAL1-10	This study
pMP3857	pENTR™/D-TOPO	*FPK1*	-	-	This study
pMP3858	pENTR™/D-TOPO	*FPK2*	-	-	This study
pMP3859	pMP2355	*FPK1*	*LEU2*	GAL1-10	This study
pMP 4062	pRS423-GAL	*MARGSH10—TEV*	*HIS3*	GAL1-10	(López-Marqués et al., 2012)
pMP4076	pENTR™/D-TOPO	*DNF3*	-	-	This study
pMP4077	pMP1965	*DNF3*	*HIS3*	GAL1-10	This study
pMP4139	pMP4062	*MARGSH10—TEV—DRS2*	*HIS3*	GAL1-10	(López-Marqués et al., 2012)
pMP4241	pMP4062	*MARGSH10—TEV—DNF3*	*HIS3*	GAL1-10	This study
pMP4429	pENTR™/D-TOPO	*GST—FPK1*	-	-	This study
pMP4430	pMP2355	*GST—FPK1*	*LEU2*	GAL1-10	This study
pMP4597	pMP4062	*MARGSH10— TEV—dnf3E342Q*	*HIS3*	GAL1-10	This study
pMP4636	pMP4062	*MARGSH10—TEV—dnf3D566N*	*HIS3*	GAL1-10	This study
pMP4637	pMP2355	*GST—fpk1K525R*	*LEU2*	GAL1-10	This study
pMP4839	pRS423-GAL	*SNAP*	*HIS3*	GAL1-10	This study
pMP4967		*DNF1* knockout cassette	*HIS3*		(Pomorski et al., 2003)
pMP4968		*DNF2* knockout cassette	*HIS3*		(Pomorski et al., 2003)
pMP4969		*DNF3* knockout cassette	*HIS3*		(Pomorski et al., 2003)
pMP5029		*DNF1* knockout cassette	*URA3*		This study
pMP5030		*DNF2* knockout cassette	*URA3*		This study
pMP5031		*DNF3* knockout cassette	*URA3*		This study
pMP5034	pMP4062	*MARGSH10—TEV—DNF1*	*HIS3*	GAL1-10	This study

pMP5036					This study
pMP5051		Cre recombinase	*LEU2*		(Pomorski et al., 2003)
pMP5052		Cre recombinase	*TRP1*		(Pomorski et al., 2003)
pMP5475	pMP4062	*MARGSH10—TEV—DNF2*	*HIS3*	GAL1-10	This study
pMP5450	pMP3129	*yeGFP-DNF3*	*HIS3*	GAL1-10	This study

[1] Abbreviations used: GST, Glutathione-S-transferase, TEV, Tobacco Etch Virus nuclear-inclusion-a endopeptidase cleavage site.[1] Abbreviations used: GST, Glutathione-S-transferase, TEV, Tobacco Etch Virus nuclear-inclusion-a endopeptidase cleavage site; *ye*GFP, yeast codon-optimized *GFP*.

Journal of Cell Science • Supplementary information

Table S3. Primers used in this study.

Name	Target	Sequence	Purpose
Primers to check deletion mutants			
OLI 3021	*dnf1Δ*	5'-CACAGAGCAAAGTCTCAC -3'	Forward to check *dnf1Δ*
OLI 3022	*dnf1Δ*	5'-CTTCTGCATCTTCACGTT-3'	Reverse in recombination region to check *dnf1Δ*
OLI 3023	*dnf1Δ*	5'-ACAACTAACGGAACCGCA-3'	Reverse in deleted section to check *dnf1Δ*
OLI 3024	*dnf2Δ*	5'-GCTGCTTCTTTCTGCTGT-3'	Forward to check *dnf2Δ*
OLI 3025	*dnf2Δ*	5'-ATCGGGTGTGCTAATATCTT-3'	Reverse in recombination region to check *dnf2Δ*
OLI 3026	*dnf2Δ*	5'-AGGGGAACGGATGCAAAA-3'	Reverse in deleted section to check *dnf2Δ*
OLI 3558	*dnf3Δ*	5'-CCAGTCTGTCAAGTGCTTTAA-3'	Forward to check *dnf3Δ*
OLI 3559	*dnf3Δ*	5'-CATAATCCTCTTCAGCAGC-3'	Reverse in recombination region to check *dnf3Δ*
OLI 3560	*dnf3Δ*	5'-GGATGGGGTTGTTTACTTTTC-3'	Reverse in deleted section to check *dnf3Δ*
OLI 3562	*HIS3*	5'-CGTTGAGTGCATTGGTGAC-3'	Reverse in *HIS3* to check knock-outs
OLI5419	*dnf1Δ*	5' CTGGGTGGTAGGGATCTATCAACTATA TTG 3'	Reverse in *Δdnf1* to check knock-outs
OLI5414	*URA3*	5' ATTGTTAGCGGTTTGAAGCAGGCGGCA GAA 3'	Reverse in *URA3* to check knock-outs
Primers for cloning			
OLI 3099	FPK1	5'-CACCATGGCTGGACACCATCACGAAC-3'	Cloning of *FPK1* in yeast plasmid forward
OLI 3101	*FPK1*	5'-TACCGACACTTATACGTCAAAGCCCCC-3'	Cloning of *FPK1* in yeast plasmid reverse
OLI3100	*FPK2*	5'-CACCATGACTCAGCAAGAAATACCG TTC-3'	Cloning of *FPK2* in yeast plasmid forward
OLI 3102	*FPK2*	5'-GAAACAATACAGAAATTTGGCCATGGG -3'	Cloning of *FPK2* in yeast plasmid reverse
OLI 3221	*DNF3*	5'-CACCGAATTCATGGGCATAGCTGATGG G CAAAGAAG-3'	Cloning of *DNF3* in yeast plasmid forward
OLI 3222	*DNF3*	5'-GTCGACTTACTCCAGATCCTTTAGCCT TGCC-3'	Cloning of *DNF3* in yeast plasmid reverse
OLI 4212	*GST*	5'-CACCATGTCCCCTATACTAGGT-3'	*GST* tagging of *FPK1* forward
OLI 4213	*GST-FPK1*	5'-GTTCATGTTCGTGATGGTGTCCAGCGTC A CGATGCGGCCGCTCGAGTCG-3'	*GST* tagging of *FPK1* reverse
OLI 4214	*FPK1*	5'-GCTGGACACCATCACGAACATGAAC-3'	*GST* tagging of *FPK1* forward
OLI 3054	*FPK1*	5'-TTATCTCTTAAAAAAGGTTCG-3'	*GST* tagging of *FPK1* reverse

Journal of Cell Science • Supplementary information

Oli5338	*loxp-URA3-loxp*	5’ TTGTTTCCACCGAAGAAACCACGCATC TGTGCGGTATTTCAC 3’	generation of *URA3* knockout-cassettes forward
Oli5339	*loxp-URA3*-loxp	5’ CGAAAGATGACGACTTTTTCTTCTGAG AGTGCACCATACCAC 3’	generation of *URA3* knockout-cassettes reverse
Oli5403	*DNF1*	5’ ATTTGTATTTTCAAGGTGGTTCTGGAAC TTTTCATGGCGATG 3’	Cloning of *DNF1* in yeast plasmid forward
Oli5404	*DNF1*	5’ CTATAGGGCGAATTGGGTACCTTAATT GTTCTGTTGTGTTCC 3’	Cloning of *DNF1* in yeast plasmid reverse
Oli5405	*DNF2*	5’ AAATTTGTATTTTCAAGGTGGTTCAAGT CCCTCCAAACCCAC 3’	Cloning of *DNF2* in yeast plasmid forward
Oli5406	*DNF2*	5’ ACTATAGGGCGAATTGGGTACTTAACG GTCCCTGCTGCGCTG 3’	Cloning of *DNF2* in yeast plasmid reverse
Oli2774	*yeGFP*	5’ GAATTCGCATGCCACGGAGTGCTTGTA CAGCTCGTCCATGCCGAGAGTGATCCC GGC 3’	Cloning of *yeGFP* in yeast plasmid reverse
oli2776	*yeGFP*	5’ CCAAAAAAAAAGTAAGAATTTTTGAAA ATTCATGGTGAGCAAGGGCGAGGAGCT GTTC 3’	Cloning of *yeGFP* in yeast plasmid forward

Primers for mutagenesis			
OLI 4512	pMP 4241	5’-GTTGAAACGATGGCTTTAGATGGCCAGAC AAATTTGAAAAGTAAACAACCC-3’	To make *dnf3*E342Q with XL Quick-change
OLI 4513	pMP 4241	5’-GGGTTGTTTACTTTTCAAATTTGTCTGGCC ATCTAAAGCCATCGTTTCAAC-3’	To make *dnf3*E342Q with XL Quick-change
OLI 4514	pMP 4241	5’-GGGCAAGTATCTTATATTTTTAGTAATAA AACCGGAACGCTGAC-3’	To make *dnf3*D566N with XL Quick-change
OLI 4515	pMP 4241	5’-GTCAGCGTTCCGGTTTTATTACTAAAAAT ATAAGATACTTGCCC-3’	To make *dnf3*D566N with XL Quick-change
OLI 4516	pMP 4430	5’-AGACGAATAGAGTGTATGCTTTGAGAGT CTTGAGTAAAGACG-3’	To make *fpk1*K525R with XL Quick-change
OLI 4517	pMP 4430	5’-CGTCTTTACTCAAGACTCTCAAAGCATA CACTCTATTCGTCT-3’	To make *fpk1*K525R with XL Quick-change
Primers for SNAP-tagging of *DNF3* at the chromosome level			
OLI 5092	*SNAP*	5’-GATTATTCAGGCAAGGCTAAAGGATCTGG AGggaggtggaATGGCTGACAAAGACTGCGA-3’	Amplification of *SNAP* with 30 bp overlap to the end of *DNF3* ORF
OLI 5093	*HIS3*	5’-CTCAATAATGTAATTAAACAAGATCACG AGAAAAATTCCCGTTTTAAGAGCTTGGTGA GC-3’	Amplification of *HIS3* cassette with 30 bp overlap to the *DNF3* 3’-UTRs
For checking Dnf3-SNAP tagging in the chromosome			
OLI 5145	*SNAP*	5’-CCTCTCCGAACTTCACCACTTTC-3’	To check fusion of *SNAP* to *DNF3*
OLI 5146	*HIS3*	5’-GTGTGGACGTTAATCACTTGCG-3’	To check integration of *HIS3* within *DNF3* 3’-UTRs
OLI 5103	*SNAP*	5’-GTGCTGTGGAAACTGCTGAAAGTGGTG-3’	To check *SNAP-HIS3* region

Reference list to SI

Alder-Baerens, N., Lisman, Q., Luong, L., Pomorski, T. and Holthuis, J. C. M. (2006). Loss of P4 ATPases Drs2p and Dnf3p disrupts aminophospholipid transport and asymmetry in yeast post-Golgi secretory vesicles. *Mol. Biol. Cell* **17**, 1632–1642.

Burgers, P. M. J. (1999). Overexpression of multisubunit replication factors in yeast. *Methods* **18**, 349–355.

Hua, Z., Fatheddin, P. and Graham, T. R. (2002). An essential subfamily of Drs2p-related P-Type ATPases is required for protein trafficking between Golgi complex and endosomal/vacuolar System. *Mol. Biol. Cell* **13**, 3162–3177.

Johnson, C., Kweon, H. K., Sheidy, D., Shively, C. A., Mellacheruvu, D., Nesvizhskii, A. I., Andrews, P. C. and Kumar, A. (2014). The yeast Sks1p kinase signaling network regulates pseudohyphal growth and glucose response. *PLoS Genet.* **10**, e1004183.

López-Marqués, R. L., Poulsen, L. R. and Palmgren, M. G. (2012). A putative plant aminophospholipid flippase, the arabidopsis P4 ATPase ALA1, localizes to the plasma membrane following association with a β-subunit. *PLoS One* **7**, e33042.

Nakano, K., Yamamoto, T., Kishimoto, T., Noji, T. and Tanaka, K. (2008). Protein kinases Fpk1p and Fpk2p are novel regulators of phospholipid asymmetry. *Mol. Biol. Cell* **19**, 1783–1797.

Pomorski, T., Lombardi, R., Riezman, H., Devaux, P. F., van Meer, G. and Holthuis, J. C. M. (2003). Drs2p-related P-type ATPases Dnf1p and Dnf2p are required for phospholipid translocation across the yeast plasma membrane and serve a role in endocytosis. *Mol. Biol. Cell* **14**, 1240–1254.

Poulsen, L. R., López-Marqués, R. L., McDowell, S. C., Okkeri, J., Licht, D., Schulz, A., Pomorski, T., Harper, J. F. and Palmgren, M. G. (2008). The Arabidopsis P4-ATPase ALA3 localizes to the Golgi and requires a β-Subunit to function in lipid translocation and secretory vesicle formation. *Plant Cell* **20**, 658–676.

Stagge, F., Mitronova, G. Y., Belov, V. N., Wurm, C. A. and Jakobs, S. (2013). Snap-, CLIP- and Halo-tag labelling of budding yeast cells. *PLoS One* **8**, e78745.

Journal of Cell Science • Supplementary information